Extensive hydro-elastic floating bridge tests: planning, design, implementation, and numerical comparison

Xu Xiang

Norwegian Public Roads Administration (NPRA, Statens vegvesen), Oslo, Norway

Correspondence: xu.xiang@vegvesen.no

Abstract

Extensive hydrodynamic and hydro-elastic tests for a long floating bridge have been carried out in the ocean basin of SINTEF Ocean for the Bjørnafjord floating bridge project. The complexity of the floating bridge plus cable-stayed bridge, in addition to its 52.58 meters model length, mark this test campaign a major undertaking in ocean basin model testing. The design, execution and analysis of the test program has been an iterative process over 5 years. The tests provide data for validation of numerical analysis, study of hydrodynamics phenomenon that cannot be well simulated by state-of-the-art engineering tools, and verification of the design under controlled environmental loads. Wave-current-structure interaction, hydrodynamic interaction between pontoons, and their impacts on hydro-elastic global responses of floating bridge (with cable stayed bridge) are the main scope of tests. Oscillation tests under different Keulegan–Carpenter (KC) numbers were also carried out for viscous drag coefficient of a pontoon in defined direction. Correlation of test results with numerical analysis is an important part of the work scope, which provides solid basis for a robust design with reduced risk. This article tries to provide an overview of the background, design, execution and correlation work of this extensive tests. Selected examples of correlation work are also provided in the article. The tests have validated the analysis method and software, provided important input to the next phase design, and enhanced the structural reliability of the bridge concept in continuous evolution.

Keywords:

Floating bridge; hydrodynamics model tests; simulation

Background

The Norwegian Government has the long run ambition to make the E39 coastal highway route of 'ferry free' standard between Trondheim and Kristiansand, Regjeringen (2017). Figure 1 illustrates all the existing fjords along this route of approximately 1100 km length. The remaining fjords to be crossed are usually wide (more than 3 km) and deep (more than 500 meters), which require new technologies and unconventional strait crossing concepts. Construction has been started for

Boknafjorden (E39 Rogfast: between Stavanger and Haugesund) which will be a subsea rock tunnel. And now the Bjørnafjord crossing is among the top of list to be realized due to its high 'social return on investment', Statens vegvesen (2020). Together with the E39 Rogfast subsea road tunnel project, Hordfast (Bjørnafjord crossing + Langenuen suspension bridge) can permanently connect Bergen and Stavanger, the second and fourth largest cities of Norway, in a region where over one million people live and create a significant part of the total export value of Norway, Mellbye et.al. (2015).

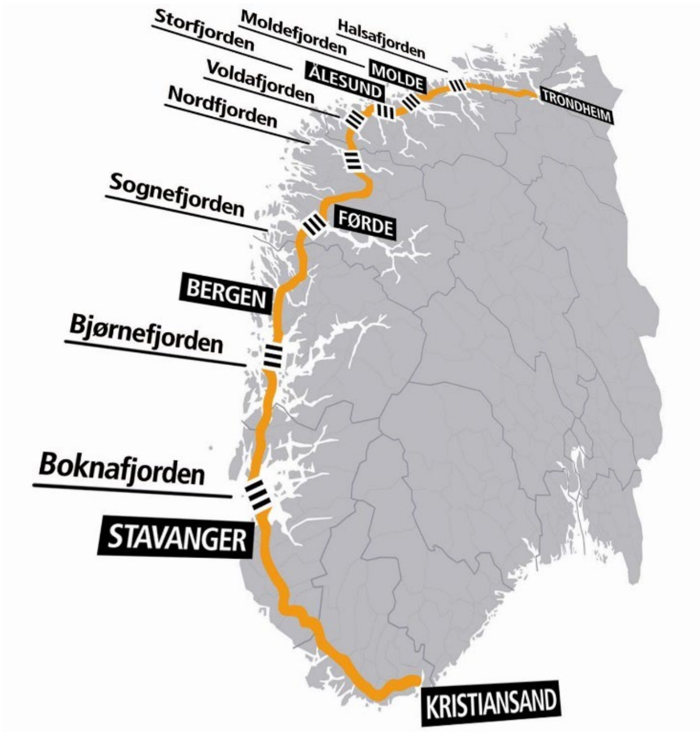

Figure 1 *The existing fjords along the E39 coastal highway route from Kristiansand to Trondheim, along the west coastal of Norway*

Engineering News-Record (2018) lists the ten longest floating bridges in the world. Among them the three longest (1988 – 2350 meters, floating part) are all located in the Seattle region of the USA. The Nordhordland and Bergsøysund floating bridges of Norway rank number seventh and eighth by the length of floating part. The Nordhordland bridge is unique among all of the installed floating bridges by including a cable stayed bridge part (founded on rock), which extended the flexibility of the whole bridge by allowing relatively large ships to pass, Aas-Jakobsen (2020). With a total length greater than 5000 meters, the Bjørnafjord floating bridge in planning will become the longest when realized. The Bjørnafjord bridge will be a completely new variant of the floating bridge based on that the floating bridge part is attached to the cabled-stayed high bridge part continuously and the transition is supported by a floating pontoon. In other words, the whole bridge girder is continuous from one end to the other end of the bridge. Figure 2 shows an artist's impression of the bridge. Different bridge components like cable stayed bridge part (with a tower and cables), bridge girder, pontoons and mooring lines are also marked in the figure. Pontoons shown in the bridge are under waves and current loads, and the distance between centerlines of two neighboring pontoons is 125m. Pontoons are connected to bridge girder via pontoon columns. In addition to the pontoons, mooring lines are also under hydrodynamic loads. All the bridge part that is above water will experience complex aerodynamic loads, which is important but not included in discussion in this article. Dynamics analysis methods of similar floating bridges under waves and current loads have been reported for either earlier phases of this bridge or earlier model tests, see Viuff (2020), Xiang et. al.(2017,2018,2019a).

The overall purpose of model tests is to verify hydrodynamics analysis theory, methods and numerical tools applied in the bridge design. The model tests were carried out also to identify hydrodynamics phenomenon that may be overlooked during the design analysis. The tests campaign is extensive, and a significant database of test results were obtained. Aside from the overview report in this article, four other articles have discussed different groups of test campaigns, Ravinthrakumar et.al. (2023a, b) (for the one and three pontoons tests) and Viuff et.al. (2023a, b) (for the high bridge hydro-elastic tests). To this article, these four articles are recommended as reference for model tests setup, model construction and other relevant tests description.

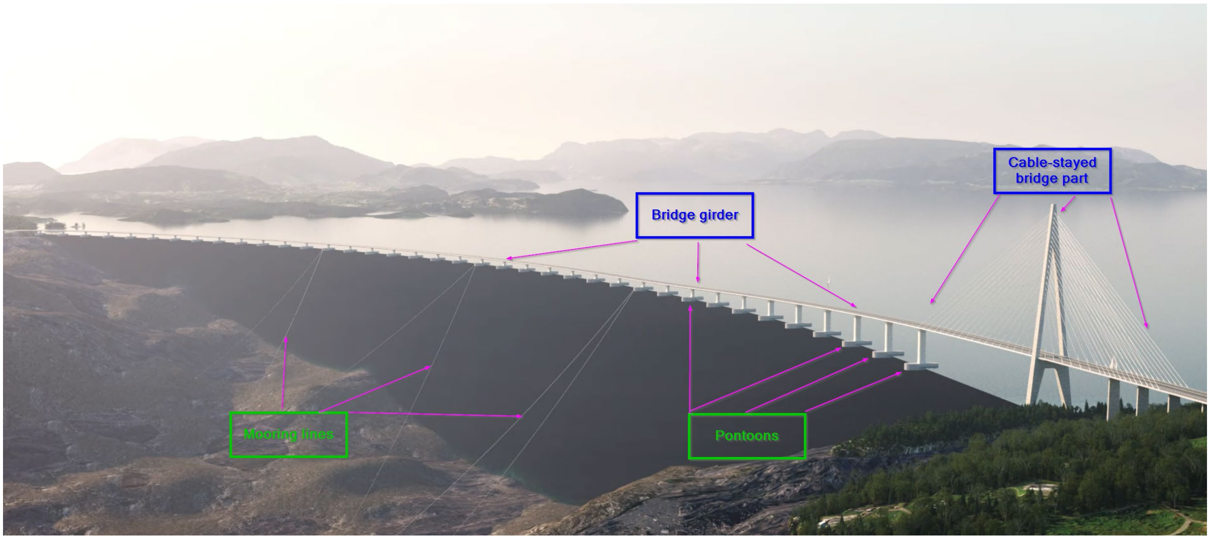

Figure 2 *Bjørnafjord floating bridge illustration: mooring lines, pontoons, bridge girder and cable-stayed bridge part (bridge girder, piers, cables and A-shaped pylon); note that the transition between cable-stayed bridge part and floating bridge part is supported by a floating pontoon (the first pontoon from left in the figure)*

Model test planning and design

The design of hydrodynamics model tests for a 5 kilometers long floating bridge is never an easy task. To the author's best knowledge, no hydro-elastic model test of this size and complexity in an ocean basin has been reported. NPRA carried out extensive model tests for the two installed floating bridges last century, Løken, et.al. (1990). The test model was for curved floating bridge without a high bridge part. The model length was 20.42m under scale of 1:40. These tests have been re-analyzed in detail by NPRA, Løken and Xiang (2018), Xiang and Løken (2019 a, b), and by the doctoral project of Viuff (2020), Viuff, et. al. (2020a, b). The most recent test campaign that is similar to the test here, was carried out by Rodrigues (2022) for a part of a straight floating bridge from the phase-3 design of Bjørnafjord floating bridge project. The main extra complexity now comes from that the new test model will include a cable-stayed bridge part, and the bridge girder is curved in the 3-D space (including the vertical direction), which brings higher requirements on position control and a larger length of test model.

Design, planning and realization of the model tests have been an iterative process over 5 years. The NPRA project has collected test requirements from the continuous bridge design, third-party review, and earlier floating bridge tests. Dedicated workshops were held in this process with our expert group and framework contract test facilities. In summary, the test design task may be answered from three aspects:

(1) What hydrodynamics parameters to be tested – choice of loads and response parameters for tests.

(2) What physical model to be tested – choice of bridge components for hydrodynamic tests and bridge part for hydro-elastic tests.

(3) Design considerations of the tests in an ocean basin – scale, similarities, environmental conditions, practical execution considerations, and so on.

What hydrodynamic parameters to be tested?

Hydrodynamic loads and responses of a long floating bridge crossing a typical Norwegian fjord are related to wave and current conditions. The bridge structural modes are usually many and in a wide range from seconds to minutes, depending on design of bridges. This means that the bridge has the potential to respond to a wide range of excitation sources from wind, waves and current, among others.

There are two main wave systems in the Bjørnafjord: locally generated wind waves and swell that penetrates from the North Sea. This is illustrated in Figure 3. The wind waves are relatively short, while the swell is much longer but low in wave height due to the ingress process via a long route from the North Sea to the intended bridge site. A typical example of 100 years wind waves is Hs = 2.1 m and Tp = 5.5s, and swell Hs = 0.34m and Tp = 14.0s, Statens vegvesen (2022). In a typical design process the wave conditions shall also be combined with current and wind. Without well documented correlation information, the 100 years waves are usually combined with 10 years current, which is according to NORSOK N-003, Standard Norge (2017).

Waves and current effects interact directly with the floating bridge through all the pontoons. This means that the pontoon hydrodynamic loads and responses are the basic parameters to be measured.

The distance between pontoons is usually in the order of around 100 meters, which may lead to hydrodynamic interaction between pontoons and further impact the loads and global responses of the bridge, Xiang et.al (2018, 2019a, 2019b). The distance between pontoon is a design issue which can be considered from both static and dynamic aspect. The gravity and wind, wave, and current induced static loads on the bridge girder between two pontoons will consume part of the girder structural capacity, while dynamic wind, waves and current induced loads will consume anther part. A preliminary study of pontoon distance optimization can be found in Giske (2019). Wave-current-structure interaction has been demonstrated to increase the loads and response on a floating bridge by model tests, Xiang and Løken (2019a, 2019b), Løken and Xiang (2018). This issue shall be studied by this new test campaign.

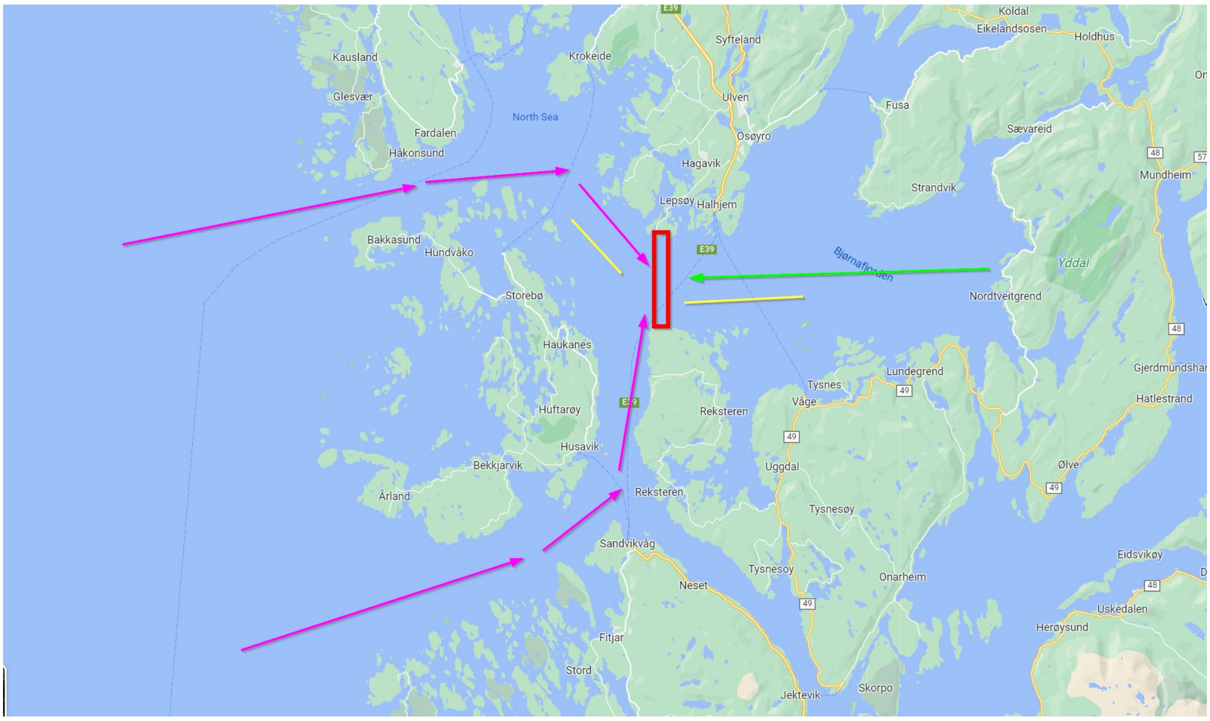

Figure 3 *Informative sketch of wave and current systems in the Bjørnafjord floating bridge site (map: maps.google.com); Pink line: North Sea swell penetration route; Green line: example of local wind waves; Yellow line: example of current route; red box: floating bridge crossing location.*

Another issue is about the hydrodynamic damping from pontoons. One may classify this damping to potential and viscous damping. The potential damping is linear and a result of wave generation when a pontoon is under forced oscillation; and the viscous damping is quadratic and related to surface friction and vortex generation of a pontoon in relative motion to the water. The typical dimensions of a pontoon (around 50 meters long, 10-20 meters width) are much less than the swell wavelength, thus little linear damping is expected at the swell period region. Damping sources like structural damping, aerodynamic damping play important roles in the floating bridge dynamic response, but usually they are not known as a prior in the design. For aerodynamic damping uncertainties come from the lack of documentation about the correlation between wind climate and the swell waves. One exemption here is for material damping: an example is that structural damping of 0.3% critical damping may be applied with relatively good safe margin for steel. Under swell wave condition the analysis results may become very conservative if no viscous hydrodynamic damping is included. Further, proper hydrodynamic viscous damping is especially important for providing right level of responses of nonlinear resonance that may happen in swell region.

Based on above discussion, the parameters to be tested shall include hydrodynamic loads and responses of pontoons and floating bridge under waves, wave-current-structure interactions, and hydrodynamic pontoon interaction conditions; the Cd (drag coefficients) of a pontoon under both static current and under different oscillation periods and amplitudes (Keulegan–Carpenter (KC) numbers); relative motions between pontoons and the water surface, and free surface elevations at selected locations.

What physical model to be tested?

Two aspects are important to answer this question. For the first what bridge components should be included in the test campaign in hydrodynamics tests of pontoons; for the second which parts of the bridge should be modelled in a hydro-elastic test of the floating bridge. The earlier test campaign in 1989, Løken et.al (1990), included a single pontoon test group and a full floating bridge tests group. Now the bridge becomes much more complex. To test the parameters defined in last section, it was decided that three groups of tests will be carried out, one for a single pontoon and one for a three pontoons system, and the third group is a hydro-elastic model of floating bridge. The environmental conditions are made similar for all groups; but for the single pontoon test group extra cases for wave-current-structure interaction and oscillation tests are added. By this way, the test results from different groups can be made comparison with.

For the first two groups pontoon tests, a natural question is how to include the influence from the rest of bridge (bridge girder, cables, tower and so on) in the model design. This influence can be considered as a very complex dynamic spring system, for which the equivalent stiffness is nonlinear and change with the dominate modes that are excited in the floating bridge. This is obvious not realistic to be realized in a single or three pontoons tests. Further, considering that the tests have hydrodynamics loads and responses as the main goal, the project group adopted a linear spring system that provides stiffness to the pontoon in two transverse and one rotational motion. The stiffness has been obtained numerically by a two-step iterative process. A static offset test in the full bridge model was carried out in different directions on a pontoon by applying different levels of loads, thus the static stiffness is obtained accordingly. The second step applies the stiffness obtained as initial value, while an iteration was carried out to fit the adjusted stiffness to allow the pontoon connected has as closest response values of the pontoon in the full bridge under selected design sea states.

For the third group, hydro-elastic tests, two design issues are most important. The first is which part of the floating bridge should be tested. Remember that the full bridge is over 5000 meters long, and even a 1:100 model means 50 meters ocean basin length. Recall that our 100 years wind waves peak period is less than 6.0 second, and for 1:100 scale this becomes less than 0.6 second in the model basin. This period is lower or on the boundary of the wave generation capacity of a typical ocean basin, for example that of Sintef Ocean (2022). Of course, wavemaker capacity is only one of many challenges if such a model is adopted. Thus, we must accept a truncated model that allows a larger scale. For better quality of waves and current conditions, the model scale should be as large as possible. But to include a larger part of the bridge in an ocean basin, the scale should be as small as possible. Final decision was based on a compromise of both and a scale of 1.31 was adopted. Half of the cable-stayed bridge part plus the first ten pontoons and the corresponding bridge girder were included in the high bridge model, Figure 22. Only one side of the cables were included in the model for simplification, but this is also based on the restrained motion of bridge girder by the earth-founded cable-tower at the tower-girder connection, where only axial motion of the bridge girder is allowed in the full bridge design. Further, the number of cables were reduced while the equivalent stiffness from the original cables was maintained. It is important to point out that the cables' top ends are connected to fixed boundary (the ocean basin wall) in the model tests, so the pylon dynamics and its impact on the floating bridge dynamics were not modelled in the model tests. This means that the cable stayed bridge modelling is not complete and does not reflect the full dynamics of the original design. All these design simplifications were analyzed and iterated many times in the model test design process. The second is how to design the boundary conditions at the truncation positions. Ideally, these could be modelled by a complex active system that tries to simulate the characteristics of the truncated part (motions, mass, stiffness, and other inertia properties). But this seems quite challenging due to the complexity of the full bridge dynamics, if not impossible. Keeping in mind that hydrodynamics tests are the core task here, we decided to avoid such a system and choose end conditions as simple as possible. The advantage of this is that quality of hydro-elastic loads and responses could be prioritized.

What special design considerations of the tests in an ocean basin?

For one and three pontoons tests, the pontoons will be attached to a rig that is again attached to the ocean basin roof. Together they form a system that may have eigen modes interacting with the measurements of pontoon motions or hydrodynamic loads. Thus, model test design must assure that the system be stiff enough, at least to a level where no eigen modes (resonance) come into the test measurements. Further, the wave and current conditions are key input to the tests and must be carefully calibrated. An important point to check here is the shape of calibrated spectrum. The target parameters are usually set as Hs and Tp, which are in principle statistical parameters of a spectrum. This indicate that different shapes of spectrum may give close Hs and Tp values. An example is shown in Figure 4 for a target JONSWAP spectrum Hs = 3.1m and Tp = 6.5s. The difference between calibrated Hs and Tp with the target is 4.2% and 0.5%, respectively. But it is obvious that the calibrated spectrum has lower energy in the frequency range of (1.5 rad/s, 2.5 rad/s), which may be related to the wavemaker's capacity of short waves generation. This indicates that calibrated wave spectrum should be applied in a correlation numerical analysis.

For high bridge tests, there are other special considerations. The test model will occupy a big part of the ocean basin water area, and some part of the model will also be attached to the ocean basin walls. This leads to two accuracy control requirements. The first is the static positions of the bridge (pontoons, bridge girder and other components) shall follow the specification with acceptable tolerance. Further, the waves and current conditions at different positions in the ocean basin (at least the positions where pontoons are located) shall be well calibrated and documented for the analysis and interpretation of test results. The re-analysis of the earlier floating bridge tests demonstrated the bridge responses are quite sensitive to a small change of wave directions, Xiang and Løken (2019). Thus, in the present tests the model is rotated in the ocean basin for achieving required wave and current directions, with the belief of better accuracy control.

Water depth is an important parameter for all three groups of tests. According to maximum depth of the Bjørnafjord (around 550m), all the possible waves to be tested are deep water waves. But there are some compromises to make for this test campaign. The first is that a higher current velocity can be generated under a smaller water depth in the ocean basin. This is needed for our highest current velocity 1.5m/s, even under the high bridge test scale of 1:31. The second is about the potential application of support structures in water. The 1989 tests applied two heavy and stiff structures at the two ends of bridge model in a water depth of 1.5 meters for holding the bridge in place. It would be an extra challenge if the present model needs a supporting structure in a water depth of 10 meters. Such a structure will be difficult to setup, heavy, flexible and may introduce unwanted uncertainties to the tests. Numerical study was carried out during the design phase by computing floating bridge responses under three different water depths: WD=550m, WD=150m and WD=75m, for both full bridge and truncated high bridge. Radiation and diffraction analysis results under different water depths were imported to the corresponding models and three hours' time domain simulations under swell (Hs =0.34m, Tp=13.5s) were carried out. Figure 5 shows standard deviation of weak axis bending moments under different conditions. It demonstrates that the water depth impact is quite small for the checked case, in addition to that the truncation effect is small for this parameter. Note here the full cable-stayed bridge is included in this computation but the model test included only half. For other parameters, the water depth effects are generally quite small, and the WD=75m leads to slightly higher responses. The model tests adopted water depths of 77.5m for the high bridge test and 62.5m for one and three pontoons tests. If one follows the definition that waves with half wavelengths smaller than the water depth are deep water waves, these two water depths guarantee waves periods less 10.0s and 9.0s are deep water, respectively.

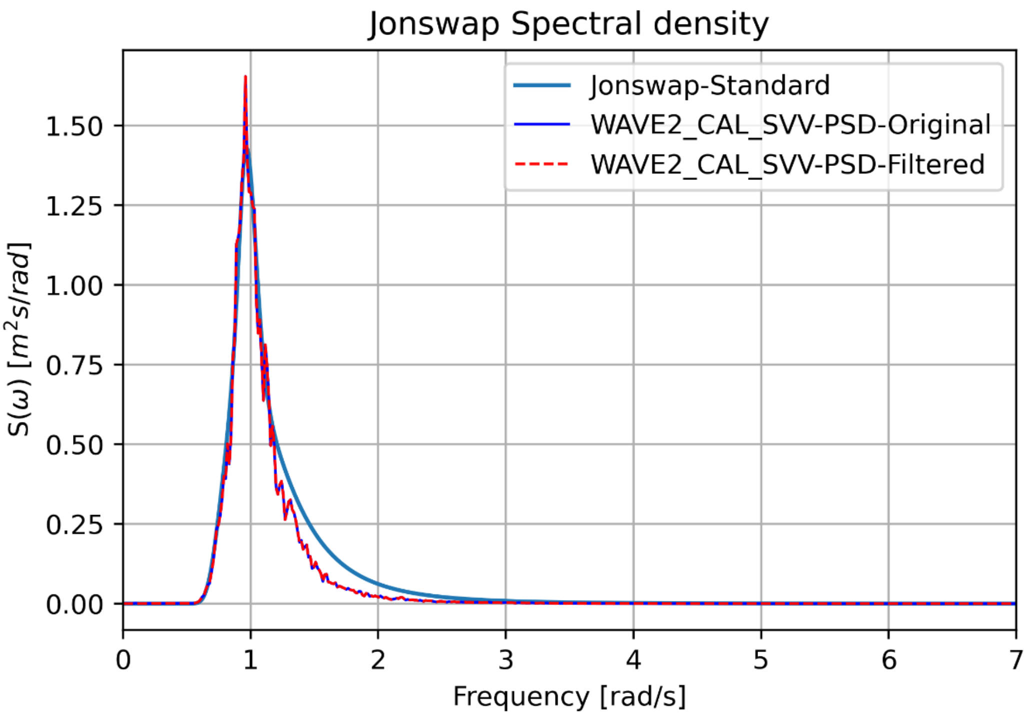

Figure 4 *Example: calibrated and standard Jonswap spectrum: target Hs =3.1m, Tp=6.5s; PSD: Power Spectrum Density.*

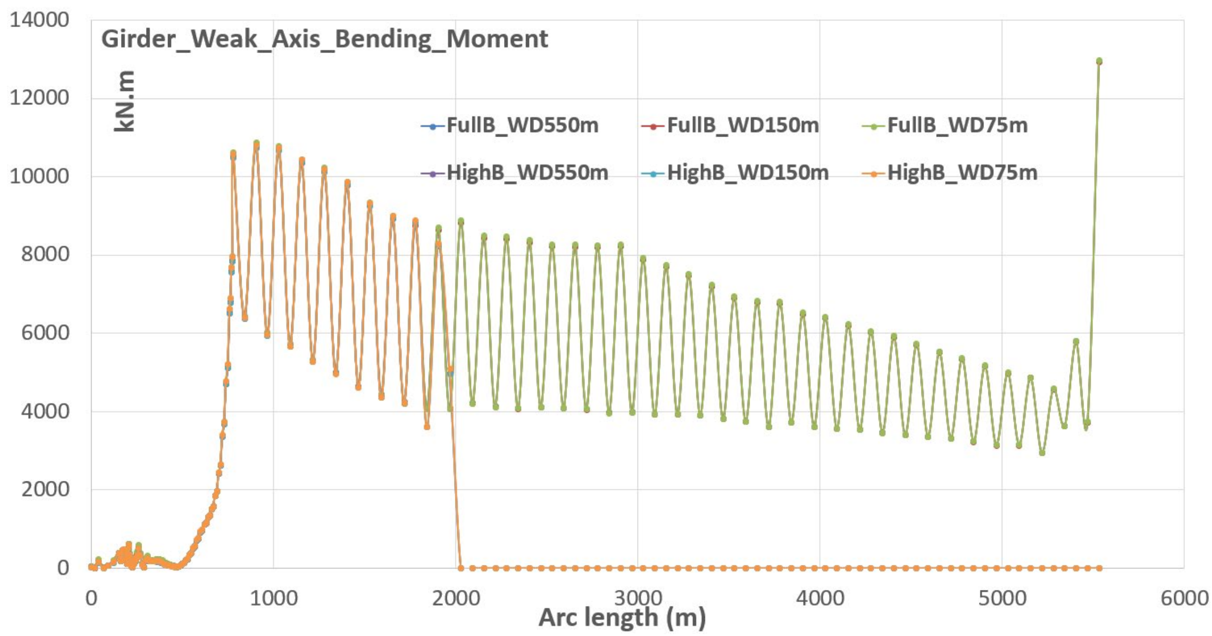

Figure 5 *Example results for weak axis bending moment (standard deviation presented): depth sensitivity of a full bridge under swell of Hs =0.34m, Tp=13.5s; FullB: full bridge; HighB: truncated bridge; for HighB the value drops to zero before 2000m where the FullB truncated;*

Model tests and analysis

Three groups of tests were carried out in the Ocean basin of SINTEF Ocean. The size of the basin is 80 m × 50 m × 10 m (length × width × depth). The ocean basin is equipped with wave generation systems on two sides as well as current generation from one side (the short side) with wave maker. More technical details of the ocean basin can be found from SINTEF Ocean (2022). The tests were so extensive that it is not practical to include all the details in this article, but they are reported separately in articles of Ravinthrakumar et.al. (2023, a, b) for single and three pontoons tests, Viuff et.al. (2023, a, b) for high bridge tests. These articles shall be read together with this article for better understanding of the test campaigns.

Similarity laws

Similarity laws assure that model test results can be applied to full scale condition. Different physical phenomena similarities are usually guaranteed by different nondimensional parameters. But it is almost impossible that all similarities can be achieved in a scaled test. Thus, it is important to decide which parameters shall be kept based on the objective of the test. Let the scale ratio be $\varepsilon = L_{model}/L_{full\,scale}$, where L is any linear dimension. The common scaling law applied is Froude number similarity for inertia scaling, and mass scaling that requires $m_{model}/m_{full\,scale} = \varepsilon^3$. Additionally, for hydro-elastic tests the elastic scaling is applied to the bridge girder:

$$[AE]_{model} = \varepsilon^3 [AE]_{full\,scale}$$

$$[GJ]_{model} = \varepsilon^5 [GJ]_{full\,scale}$$

$$[EI]_{model} = \varepsilon^5 [EI]_{full\,scale}$$

Here EA, EI and GJ are axial, bending, and torsional stiffnesses of the bridge girder. However, it will be quite challenging to satisfy all these scaling at the same time in the girder modelling. The final decision was to focus on the bending and torsional stiffness scaling of the girder, while the axial stiffness of the model was around 30 times higher than the original bridge. An axial spring is attached to the boundary condition at the floating bridge end to account for this change. Details on girder modelling are documented in Viuff et.al. (2023a).

For the viscous effects to be similar between model and prototype, the Reynolds number must satisfy $[UL/\vartheta]_{model} = [UL/\vartheta]_{full\,scale}$, where U is a representative fluid velocity and ϑ is the fluid kinematic viscosity. This is almost impossible to be achieved in relevant hydrodynamic tests. Turbulence triggering mechanism is usually applied to ensure that the tests are under turbulence as in the full scale, thus, to reduce the scale effect, Faltinsen (2005).

One pontoon and three pontoons tests

The first group 'single pontoon tests' and second group 'three pontoons tests' were carried out under scale of 1:25 (WD =62.5 m). Figure 6 and Figure 7 show one and three pontoons tests in the basin. Figure 8 describes coordinate systems. All pontoons use a global coordinate system OXYZ that coincides with the mid-pontoon (pontoon-2) local coordinate system at static condition. A standard right-hand coordinate local system $o_i x_i y_i z_i$ (i=1,2,3) is defined for each pontoon with y_i-axis in transverse direction and x_i axis in the length direction of the pontoon, z_i-axis pointing upwards with $z_i = 0$ in the waterline. The global direction of waves and current is defined by the angle from the positive X-axis to the (going towards) direction of the waves (current) using right hand principle. This gives 0-degree direction in positive X-axis and 90 degrees in positive Y-axis. Note that for high bridge tests different coordinate systems are applied for different components.

In these two groups, loads and motions of one pontoon or three pontoons under different regular and irregular waves with or without current were tested. In Figure 7 the central pontoon is connected to a flexible stiffness system which can be locked in fixed condition tests for excitation loads. The pontoon in the center is named pontoon-2 and the other two pontoons as pontoon-1 and pontoon-3. For one pontoon tests the same rig setup was used by removing only the two side pontoons which were fixed under three pontoons tests. Pontoon geometry is composed of two half circles (with same diameter as the pontoon width) at two ends and a rectangular in the middle. The pontoon-2 dimensions and stiffnesses in x-, y-, and Ry- directions in the tests are listed in Table 1 and Table 2. Wave probes are setup around the center pontoon and on the pontoon. Oscillation tests of a pontoon different KC numbers were also tested for the purpose of extracting viscous damping coefficient in the direction of oscillation, and this is referred to Ravinthrakumar et. al. (2023a).

	Unit	**Dimension**
Length	m	53
Width	m	14.9
Radii ($r_{2,yy}$)	m	18.145
($x_{2,CoG}$, $y_{2,CoG}$, $z_{2,CoG}$)	m	(0, 0, 0)
Draft	m	5.0
Freeboard	m	3.5
Displacement	m^3	3710.281

Table 1 *Main dimensions for the center pontoon; the pontoons 1 and 3 have the same geometry and displacement but are fixed in three pontoons tests*

Stiffness in DOF	**Stiffness**
Kxx (translational spring along the x_2 axis)	4.6944E+03 (kN/m)
Kzz (translational spring along the z_2 axis)	1.1740E+03 (kN/m)
Kry (rotational spring around the y_2 axis)	2.5770E+04 (kN.m/degree)

Table 2 *Required stiffnesses for the connection system (of pontoon-2) in motion tests*

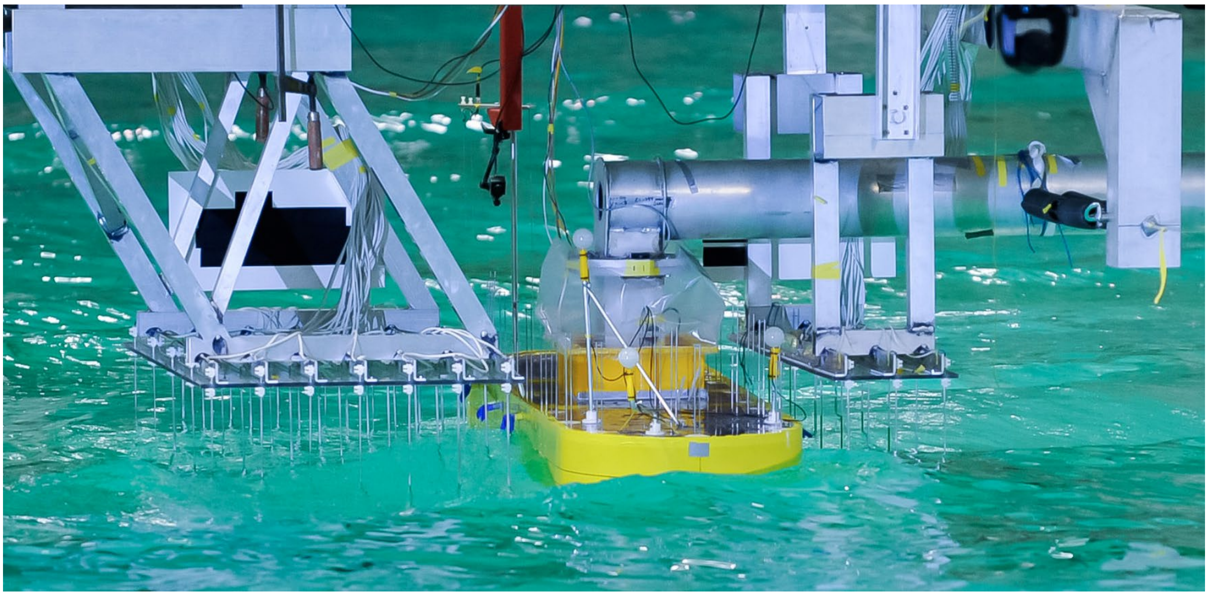

Figure 6 *Single pontoon tests, wave testing; scale 1:25, WD=62.5m; The instrumentation includes stiffness rig, motion tracking system, wave probe arrays at each side of pontoon and green water probes mounted to the pontoon deck*

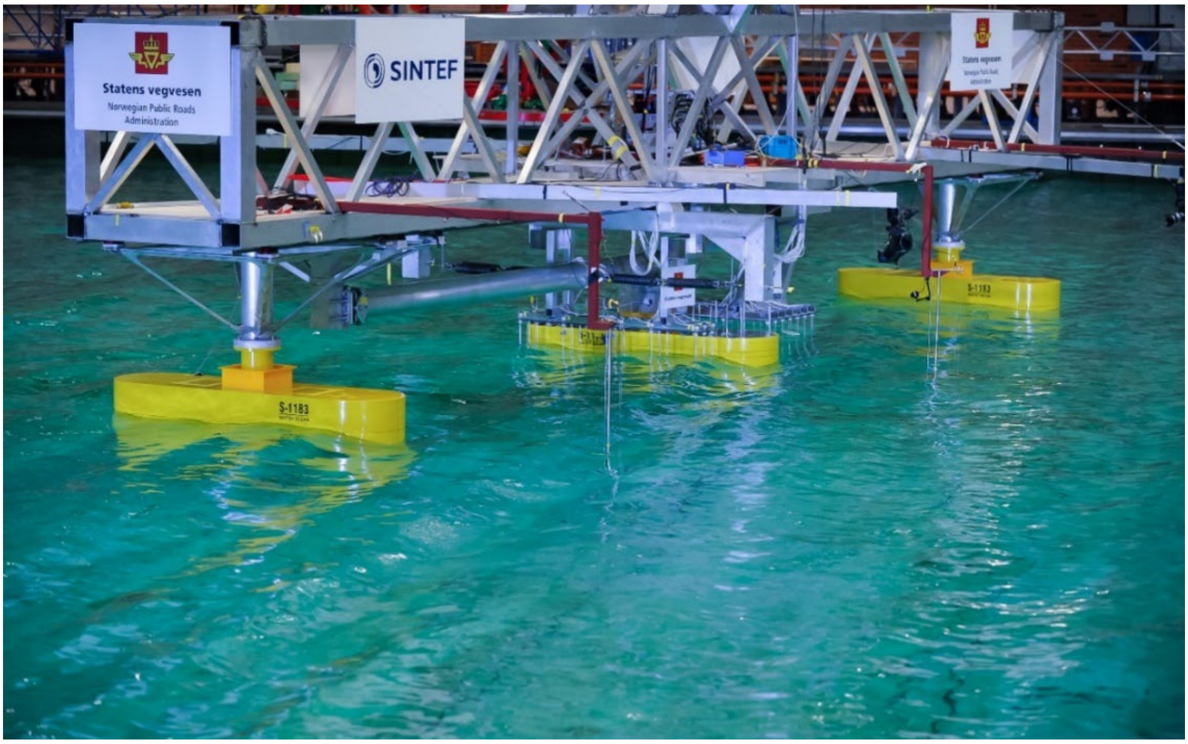

Figure 7 *Floating bridge model tests - three pontoons tests; note that for one pontoon tests the same setup was used by only removing the two side pontoons which were fixed under tests*

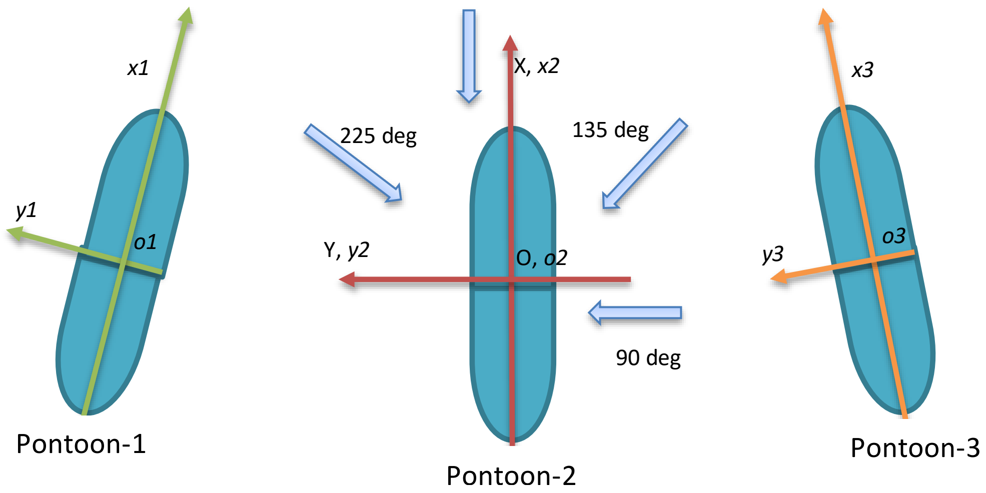

Figure 8 *Global(OXYZ) and local coordinate systems to three pontoons; note that Pontoon-1,3 are removed during single pontoon test*

One pontoon and three pontoons tests – numerical comparison

Different types of numerical models have been setup for comparison between model tests and computations. OrcaWave were applied to compute basic hydrodynamic coefficients, Response Amplitude Operators (RAOs) of wave excitation loads and wave elevations at specified points. OrcaFlex was applied to compute motions under both regular and irregular waves in the time domain. The measured waves at reference point in ocean basin are applied as input in all OrcaFlex simulations. For cases with (waves + current), some computations were also carried out in a Rankine-source-based time domain software DNV-Wasim for wave loads. The comparison is extensive and only results from regular wave cases under zero current will be discussed here.

For pontoon motion computations there are two ways of specifying the stiffness. One way applies directly a stiffness matrix based on values given in Table 2; while a more complete way models the whole test rig structure shown in Figure 9.The pendulum rig is composed of a stiff tube structure supported by three springs (one vertical and two horizontal). It is allowed to rotate about an end universe joint in up-down and sideways directions, but not allowed to have torsional motion. The pontoon pitches about a hinge at the waterline of the model. The full rig OrcaFlex model is presented in Figure 10. And the modelling follows the details of rig setup in the model test report, SINTEF Ocean(2020a). The pretension of the springs, and the stiffness applied at the pontoon reference point (local coordinate system at the free surface) can be checked by static tests in the OrcaFlex model similar to the wet pull test in the model basin. The eigen periods of the system can also be check by modal analysis, which is an iteration process. In all the computations in OrcaFlex for motions of 1 and 3 pontoons tests, Cd = 0.75 was applied to x- and y- direction, and Cd =4.1 to the z- direction.

The six linear excitation loads on pontoon-2 under the wave direction of 220 are compared from Figure 11 to Figure 16. Loads from calculation and model tests of both single and three pontoons are compared. The comparison is generally good for both one and three pontoon cases. It is demonstrated by the comparison that hydrodynamic interaction effects on the wave loads are not negligible and can be well captured by a panel model method. Further, comparing the peak locations and amplitude between model tests and computation, one can confirm that the resonances produced by hydrodynamic interaction are mostly physical, and the peak values predicted are on the right level. This indicate no extra damping is needed for numerical prediction on this for engineering design.

First order pontoon-2 motions are compared from Figure 17 to Figure 19 under wave direction of 220. The comparison between model tests and computations have demonstrated clear effects of hydrodynamic interaction on the motion responses of the center pontoon, especially in the heave direction. For surge and pitch motions are effects less prominent. In addition, the computation by full-rig model provides better comparison with model tests than the simple (frequency + stiffness) model, indicating that the hydrodynamic interaction effects are coupling with the (nonlinear) mechanical properties of the rig system.

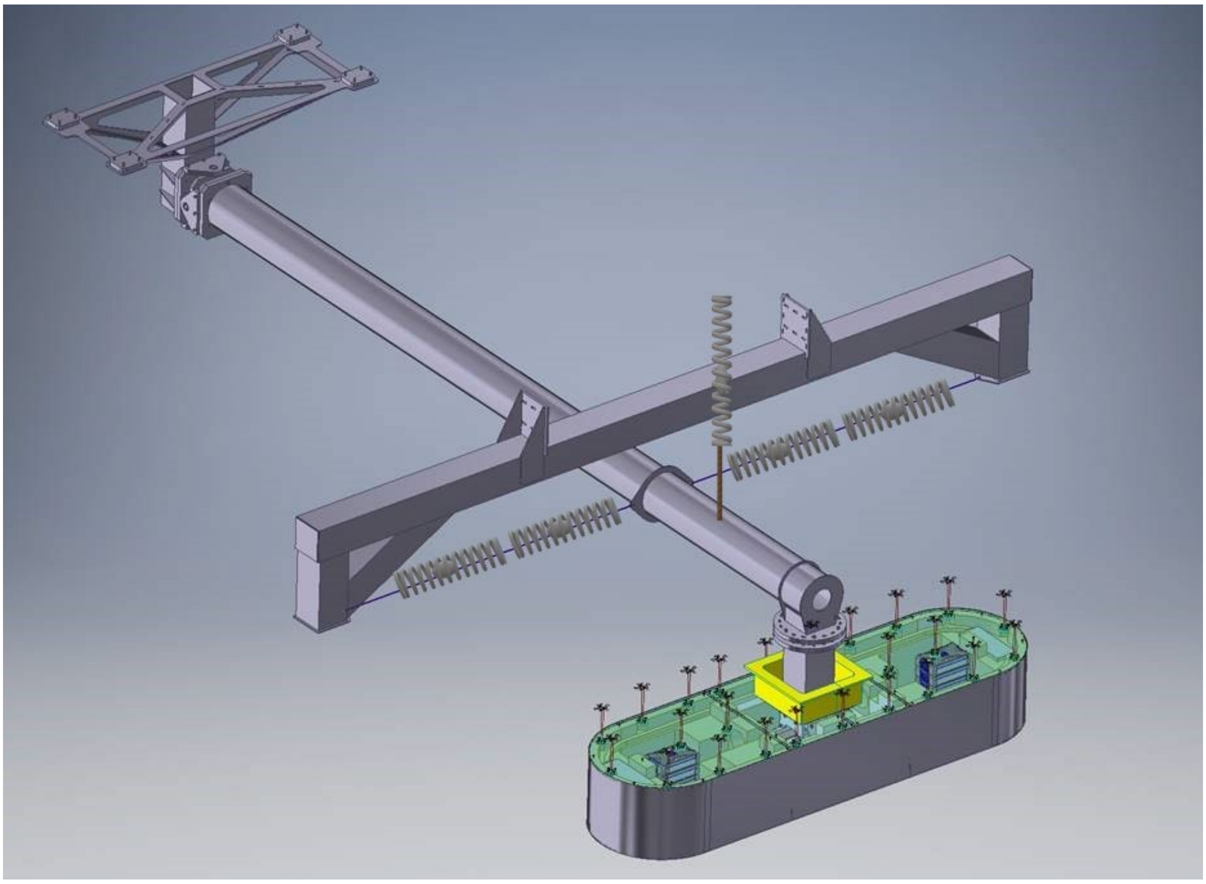

Figure 9 *Pontoon attached to the pendulum rig. The pendulum is allowed to rotate about the universal joint (up-down, sideways). Torsional motions are prevented. The pontoon pitches about a hinge at the waterline of the model (5 m above baseline, full scale).*

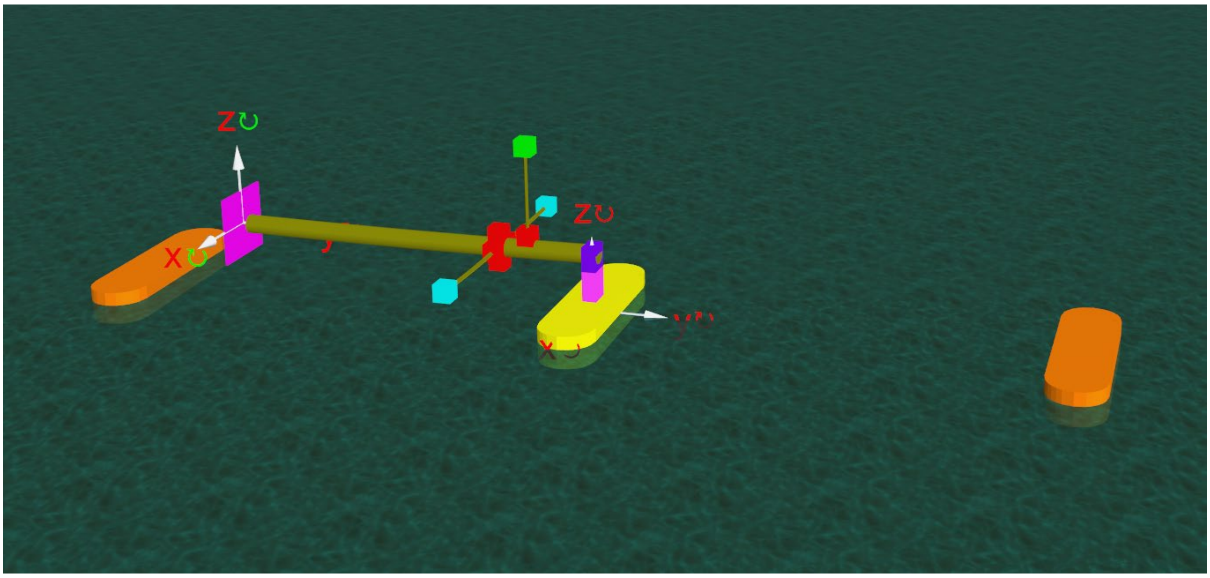

Figure 10 *OrcaFlex model of the flexible rig system in the model tests – 3 pontoon tests; the springs are modelled as equivalent wires; Note that the same rig setup applies to 1 pontoon tests*

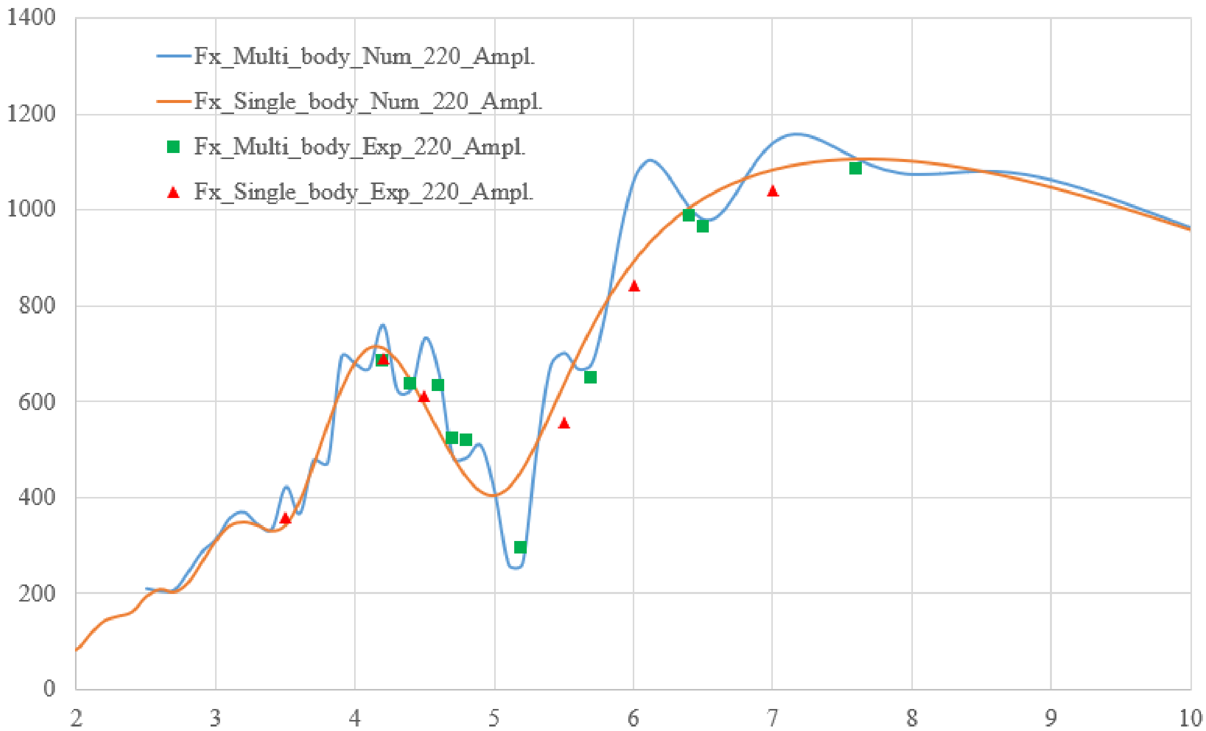

Figure 11 *First order wave loads RAOs on the pontoon, with/wo hydrodynamic interaction, model tests comparing with numerical results (SVV, by OrcaWave); wave direction = 220-degree,* x_2*- force. x axis: wave period in second, y axis: RAO in kN/m*

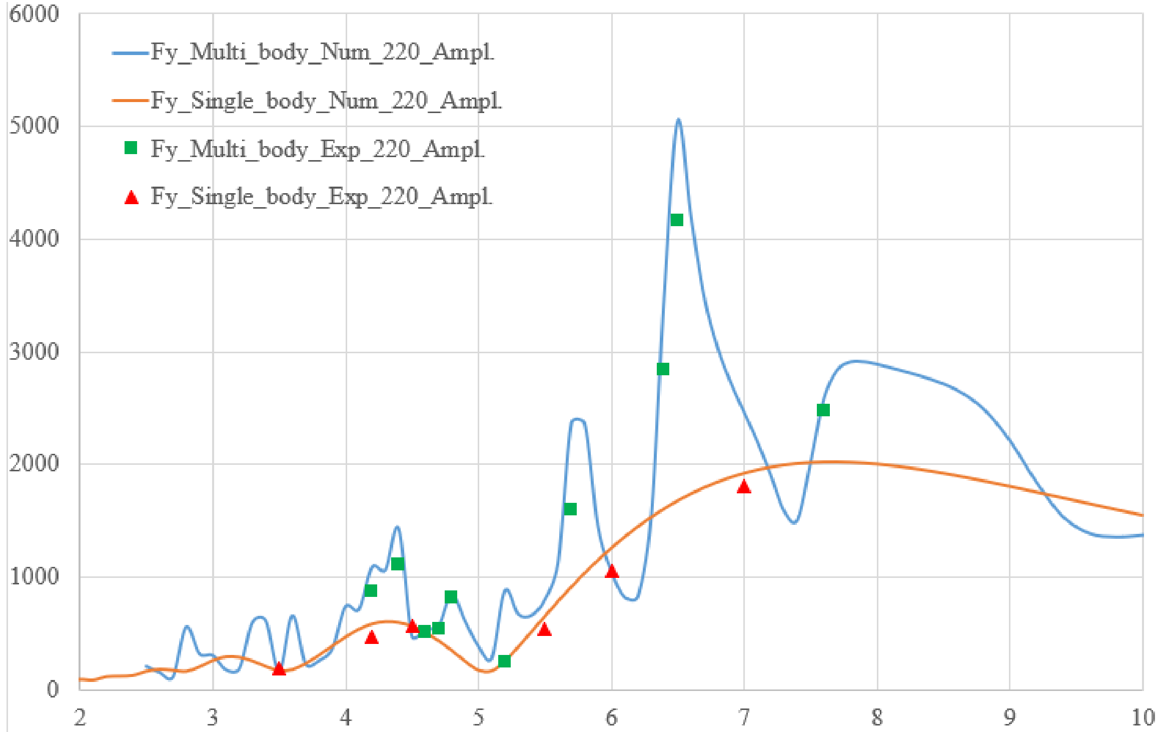

Figure 12 *First order wave loads RAOs on the pontoon, with/wo hydrodynamic interaction, model tests comparing with numerical results (SVV, by OrcaWave); wave direction = 220-degree, y_2-force. x axis: wave period in second, y axis: RAO in kN/m*

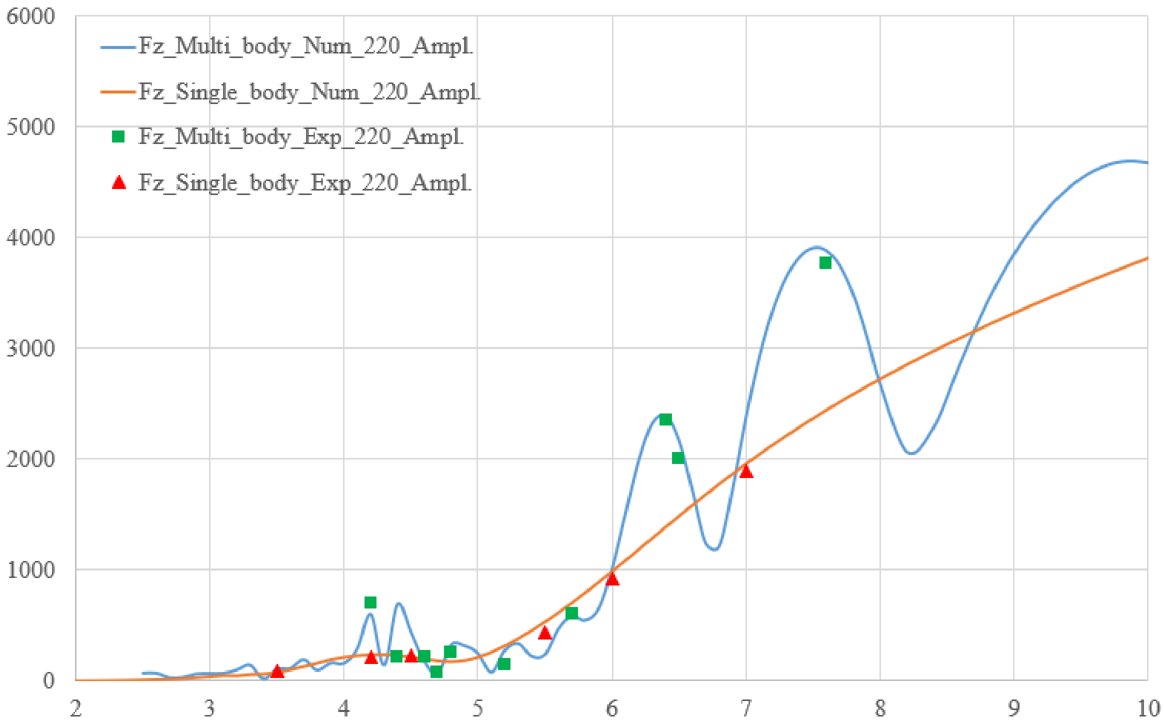

Figure 13 *First order wave loads RAOs on the pontoon, with/wo hydrodynamic interaction, model tests comparing with numerical results (SVV, by OrcaWave); wave direction = 220-degree, z_2- force. x axis: wave period in second, y axis: RAO in kN/m*

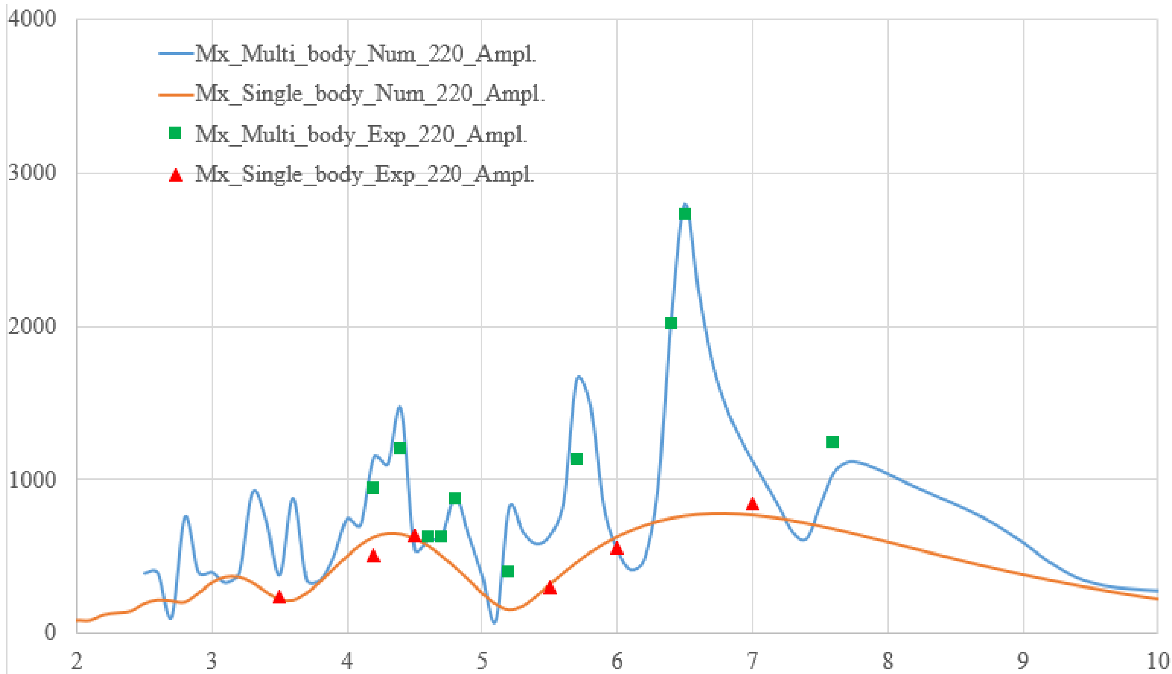

Figure 14 *First order wave loads RAOs on the pontoon, with/wo hydrodynamic interaction, model tests comparing with numerical results (SVV, by OrcaWave); wave direction = 220-degree, Rx_2-moment. x axis: wave period in second, y axis: RAO in kN.m/m*

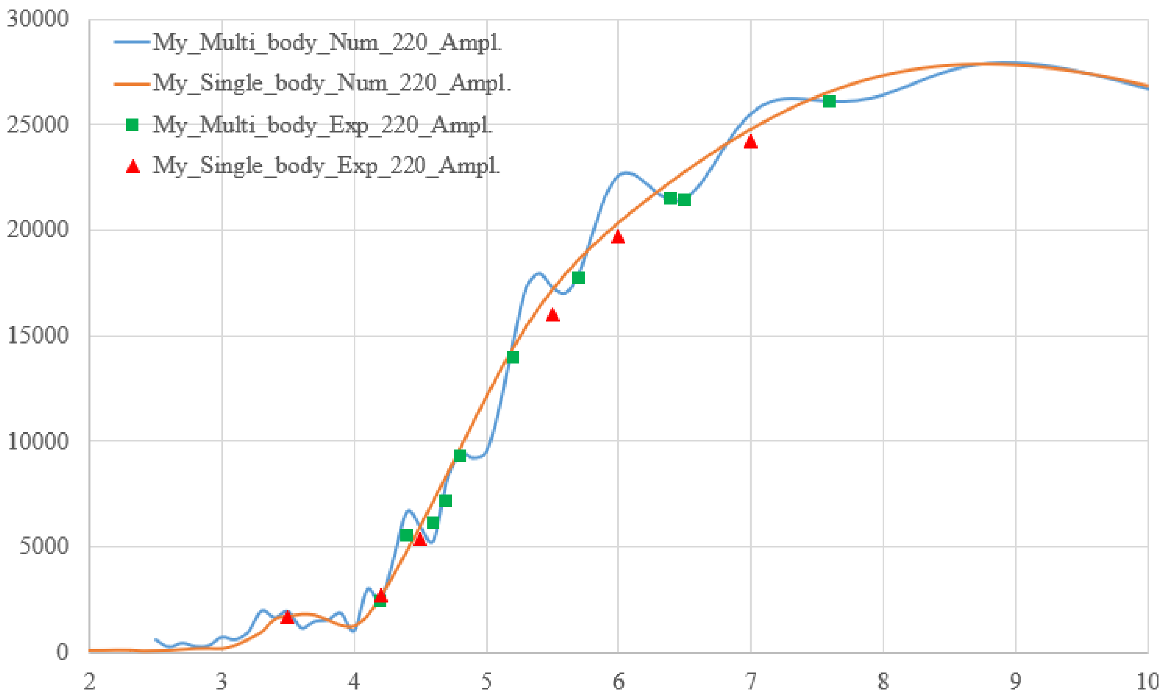

Figure 15 *First order wave loads RAOs on the pontoon, with/wo hydrodynamic interaction, model tests comparing with numerical results (SVV, by OrcaWave); wave direction = 220-degree, Ry_2- moment. x axis: wave period in second, y axis: RAO in kN.m/m*

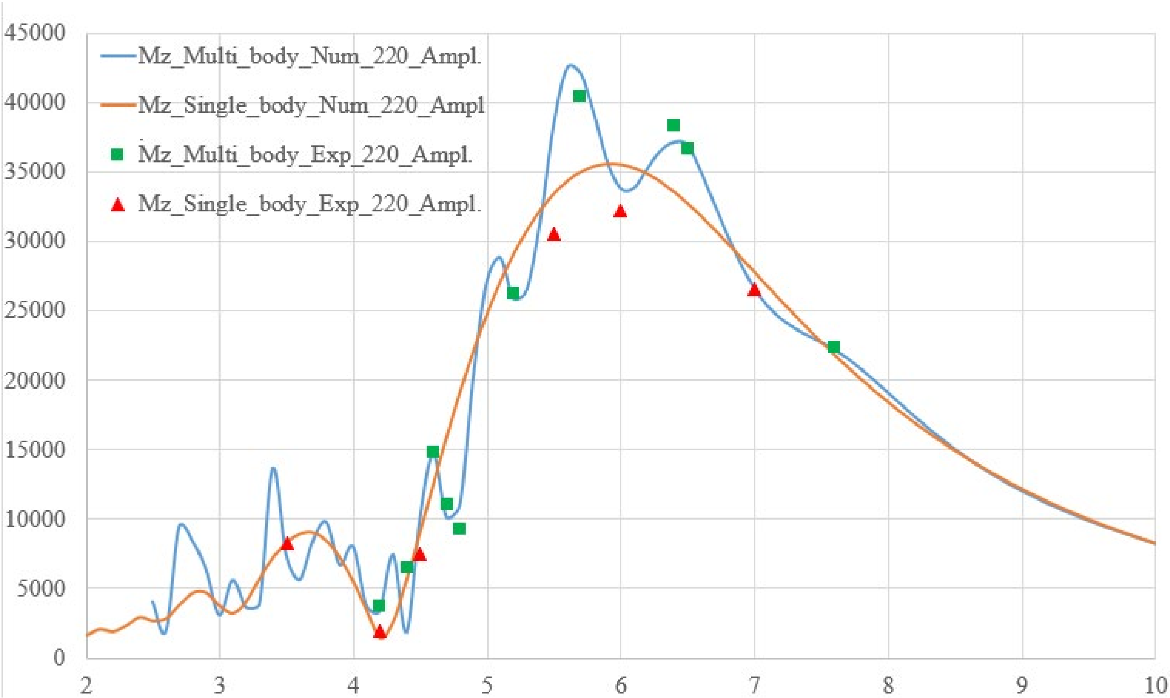

Figure 16 *First order wave loads RAOs on the pontoon, with/wo hydrodynamic interaction, model tests comparing with numerical results (SVV, by OrcaWave); wave direction = 220 degree, Rz*$_2$*-moment. x axis: wave period in second, y axis: RAO in kN.m/m*

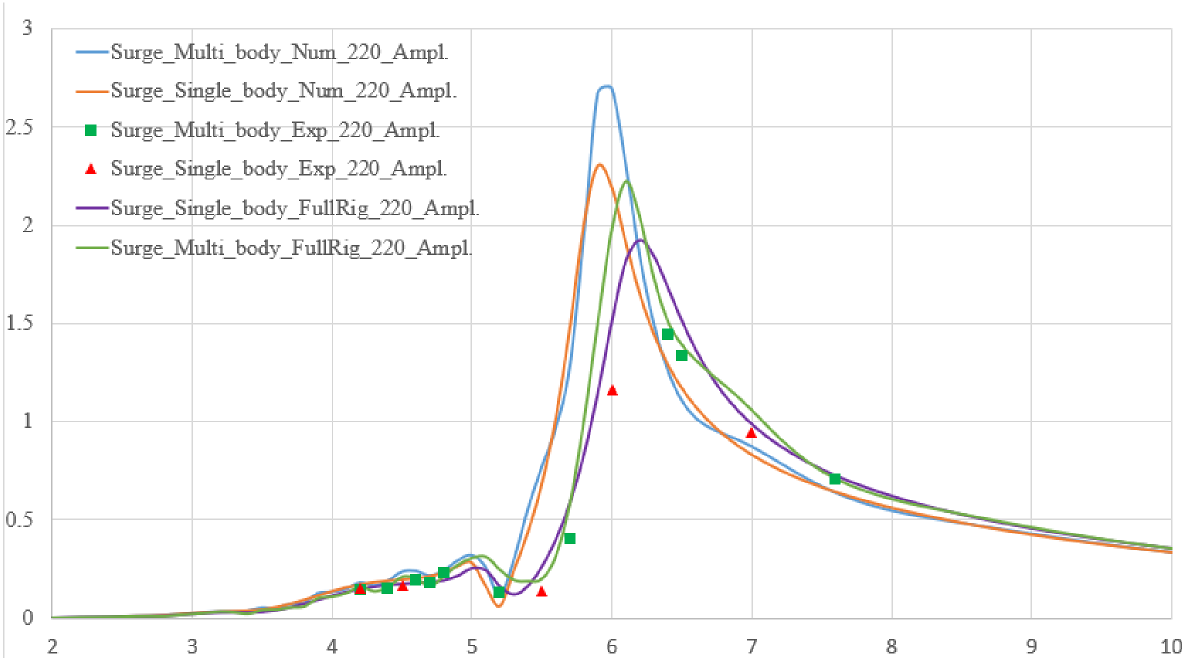

Figure 17 *First order motion RAOs on the pontoon, with/wo hydrodynamic interaction, model tests comparing with numerical results (SVV, by OrcaWave); wave direction = 220 degree,* x_2 *motion/surge. x axis: wave period in second, y axis: RAO in m/m*

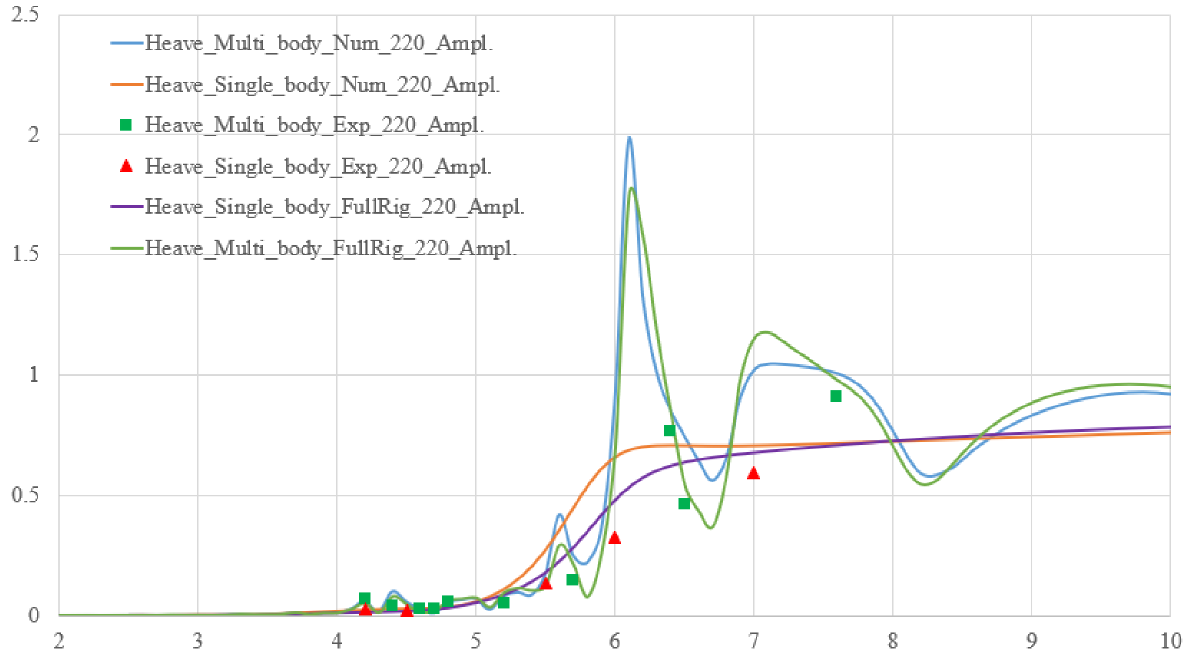

Figure 18 *First order motion RAOs on the pontoon, with/wo hydrodynamic interaction, model tests comparing with numerical results (SVV, by OrcaWave); wave direction = 220 degree,* z_2 *motion/heave. x axis: wave period in second, y axis: RAO in m/m*

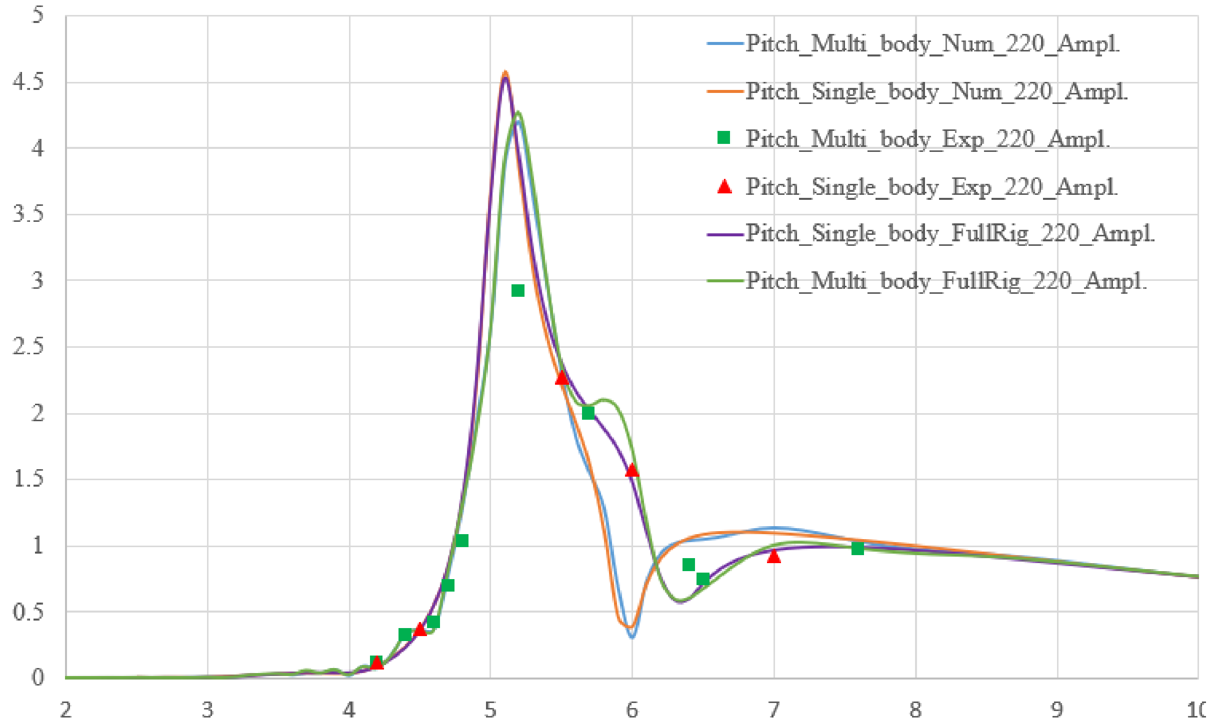

Figure 19 *First order motion RAOs on the pontoon, with/wo hydrodynamic interaction, model tests comparing with numerical results (SVV, by OrcaWave); wave direction = 220 degree,* Ry_2 *motion/pitch. x axis: wave period in second, y axis: RAO in degree/m.*

Hydro-elastic high bridge tests

The third group 'high bridge tests' was carried out under scale of 1:31 (WD =77.5 m). The test model is composed of a cable-stayed bridge part and floating bridge part. In total 10 pontoons were included in the model. Only half of the full cable-stayed bridge is included in the model based on the dynamic properties of the original bridge, and the model test design after tremendous amount of analysis and screening, Xiang and Løken (2020c). Different wave and current directions were realized by rotation of the bridge model in the ocean basin. In total 3 different configurations were tested during the campaign, which includes six wave directions with or without current combined. Since current generation is only possible from one side, colinear wave and current conditions are not possible for all the directions. Control of environmental conditions modelling was given high priority during the test planning and executions. Groups of wave probes were mounted at all pontoon positions and selected reference points during calibration and test runs. Current variation has also been documented a crossing the ocean basin. These can provide information of inhomogeneity of waves and current in the basin. All the structural properties and modelling details of the floating bridge test model can be found in Viuff et.al. (2023, a) and will not be repeated here.

A series of cross-sections along the bridge girder are used to describe the bridge girder's curvature and position in the space. The right-hand coordinate system $o_{bg,k}x_{bg,k}y_{bg,k}z_{bg,k}$ is applied to define the k_{th} bridge girder cross-section, as shown by Figure 20 of a bridge section in which a pontoon and a column are also included. The whole bridge girder in the test has a uniform cross-section. The origin of each section system is always the cross point of two neutral axis ($x_{bg,k}$ *and* $y_{bg,k}$ *axis*) to the section, while $z_{bg,k}$ is perpendicular to the plane defined by them. The origin of the cross-section system $o_{bg,k}$ follows the continuous curve from one end (End-1) of the girder at bridge tower to the other end at the floating bridge (End-2). Right-hand coordinate local system $o_ix_iy_iz_i$ (i=1,2,3…10) is defined for each pontoon with x_i-axis in transverse direction and y_i axis in the length direction of the pontoon, z_i-axis pointing upwards with $z_i = 0$ in the waterline. Note that the pontoon coordinate systems are different in high bridge tests and the single/three pontoons tests, Figure 8.

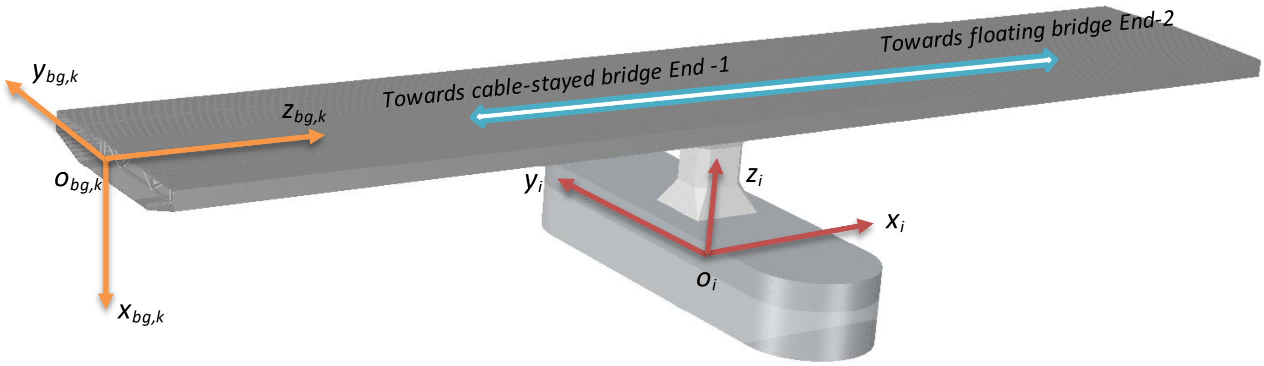

Figure 20 *Bridge girder coordinate system* $o_{bg,k}x_{bg,k}y_{bg,k}z_{bg,k}$ *in a bridge section with pontoon and column; shown in the figure also an example of pontoon coordinate system; At where pontoon column is connected to the bridge girder, the* $y_{bg,k}$ *is pointing in the same direction as the* y_i *direction of the*

pontoon coordinate system; The figure also shows the directions of girder towards cable-stayed bridge and floating bridge ends

The installed bridge model under one configuration is shown in Figure 21. The cable stayed part is on the left-hand side, with cables attached to the basin wall. Figure 22 provides explanations about different bridge components of the model. Figure 23 sketches different components of the model with section and ballasting information. The bridge girder is varying as a 3D curve that starts from Sec-0 (arc length = 0 m) and ends at Sec-16 (arc length = 1630 m). The first pontoon (Pontoon-1) connects to the girder at Sec-6 (arc length =380m) via pontoon column-1; the arc length difference between each pontoon column connection point on the girder is 125 meters. Two symmetrical groups (5 cables in a group) of cables are connected to the bridge girder between Sec-0 and Sec-6. Each group of cables are named as Cb_Fx5, Cb_Fx9, Cb_Fx12, Cb_Fx15 and Cb_Fx18, where x can be E (east) or W (west). The other ends of all the cables are connected to the tower (basin wall).

The measurements were carried out for: 6 DoF motions for 10 pontoons, bridge girder sectional loads (6 DoF at two ends; 5 DoF at 10 locations), motions (3DoF at 13 locations) along the bridge girder, and cable tensions in 10 cables. Definitions, coordinate systems and how these parameters are named in results comparison are given in Table 3. Loads in pontoon columns and relative motions between pontoons and waves were also measured, but these will not be reported here.

Components	Measurements and presenting names in results comparison
Pontoon motions	Pontoon 6 DoF motions - translational Pontoon x, y, z motions in local x_i, y_i, z_i directions, rotational Pontoon Rx, Ry, Rz motions around axis x_i, y_i, z_i; measured for all pontoons; refer to coordinate system in Figure 20
Girder motions	Girder 3DoF motions – translational Girder x, y and z motions in $x_{bg,k}$, $y_{bg,k}$ *,and* $z_{bg,k}$ directions; measured at 13 positions along the girder; refer to coordinate system in Figure 20
Girder loads	Girder 6 DoF loads – shear and axial forces Girder x(v), y(t), z(a) forces in $x_{bg,k}$, $y_{bg,k}$ *,and* $z_{bg,k}$ directions; bending and torsional moments Girder Mx, My, Mz moments around $x_{bg,k}$, $y_{bg,k}$ *,and* $z_{bg,k}$ axis; 6 DoF loads measured at two ends (END1 and END2); 5 DoF loads (without axial force along $z_{bg,k}$) loads measured along the bridge girder at 10 locations; refer to coordinate system in Figure 20
Cable tension	Cable tension Cable tension – East or West measured for 10 wires divided to two groups (Cb_Fx5, Cb_Fx9, Cb_Fx12, Cb_Fx15), x =E or W

Table 3 *Measurements and presentation names in results comparison in the high bridge tests*

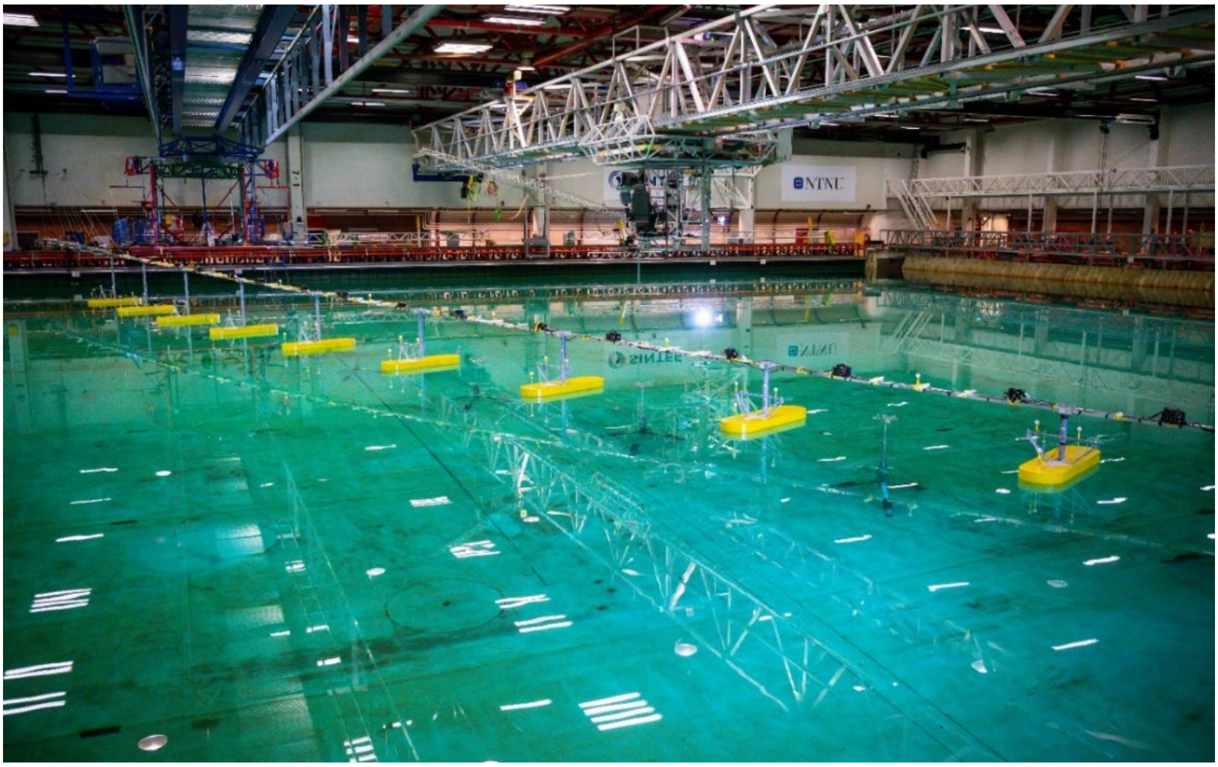

Figure 21 *Floating bridge model tests - high bridge tests;*

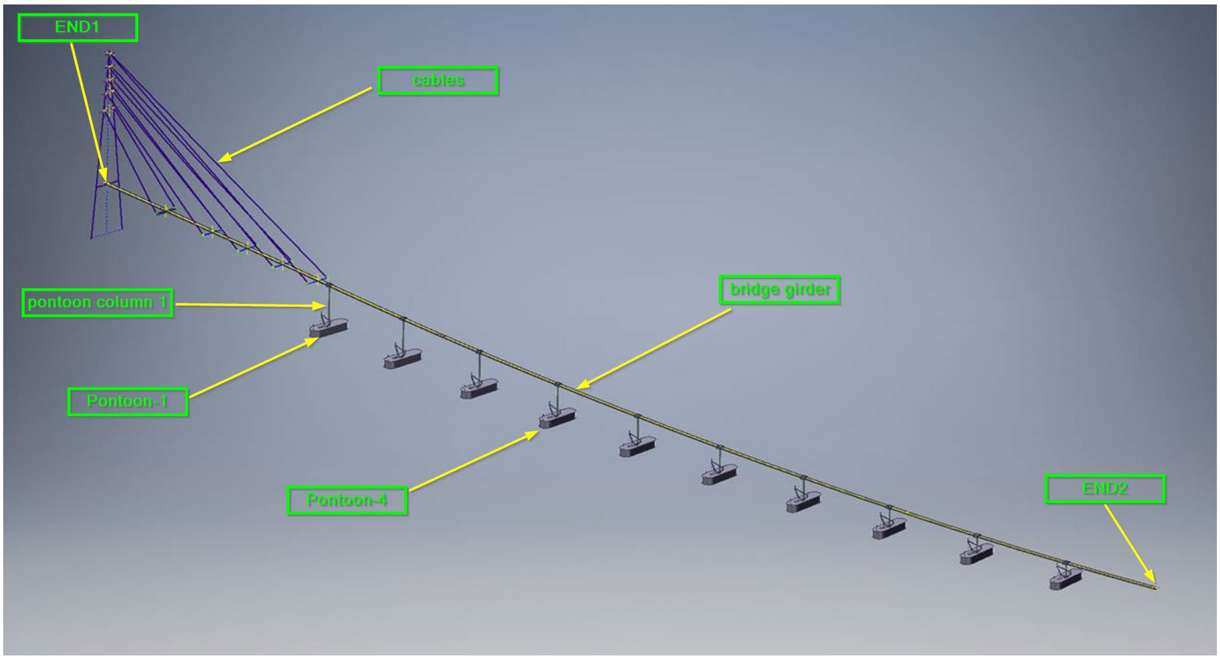

Figure 22 *Floating bridge high bridge test model with names to different parts.*

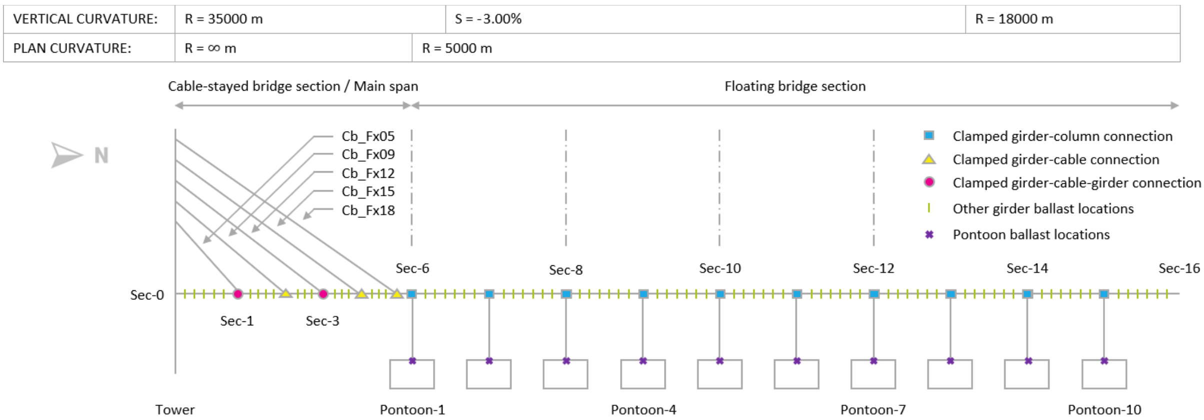

Figure 23 *Overview of floating bridge model with relevant nomenclature, Sintef Ocean (2021)*

Hydro-elastic high bridge tests – numerical comparison

An OrcaFlex model was setup during the model tests given all the details of the physical bridge model in the ocean basin. The model is used to simulate the test cases in the time domain applying the measure waves at the reference position of the wave calibration. The wave tests without current can be simulated directly. However, simulation of the tests with both waves and current are more challenging. Dispersion relation under refraction effects of waves running on a current changes wave length, Svendsen (2005). Analysis of model test wave calibration data has also documented the wavelength change due to wave current interaction, Xiang (2023). This has two consequences for floating bridge response analysis: locally (for a single pontoon) and globally (for the hydro elastic bridge). Locally, the change of wavelength leads to change of e.g., pressure distribution on a floating bridge pontoon, and consequently the wave excitation forces and other hydrodynamic coefficients. Globally, the change of wavelength changes the relative phase between pontoons, thus the global responses of the floating bridge. The wave-current interaction problem is dependent on current speed, wave periods, and relative direction between the current and waves. How to implement these shall be carefully studied, and we leave it for future report. Only waves with zero current cases simulations are to be included in this article.

The OrcaFlex model applies input from OrcaWave for pontoon potential flow hydrodynamics coefficients. Pontoons experience viscous hydrodynamic loads under relative motions to water. The load can usually be modelled as a Morison type drag load with coefficient from literature or model tests. This load is considered important for bridge responses under swell cases, where potential damping level is low. An important note here is that Morison model seems not working correctly in application in the wave-current-interaction cases, where a damping effect from current to the bridge response may be expected, while observation in model tests always shows an increase of the responses. This observation is also documented in Xiang and Løken (2019a, 2019b). As explained above, this is mainly due to that wave-current-interaction is not properly accounted for. In the numerical model, Morison drag force is applied to the pontoon in local x-, y- and z- directions.

Coefficients applied are listed in Table 4. According to numerical tests, the bridge responses are more sensitive to the value of drag in y- direction. A sensitivity test was carried out for this direction around the value (Cd_y = 0.75) which was the lowest Cd_y coefficient obtained from the oscillation tests of a single pontoon at under KC number in the range of (1,30). Cd_x and Cd_z are set to 1.50 and 4.10 after some trial correlation with the model tests. Shao et.al. (2019) provides some technical reference of the Cd_z=4.10 selection.

ID	Cd_x	Cd_y*	Cd_z
CD0	1.50	0.50	4.10
CD1	1.50	0.75	4.10
CD2	1.50	1.00	4.10
Reference Group**	0.00	0.00	0.00

Table 4 *Morison drag coefficients for the pontoon viscous loads; *: values for sensitivity study on drag coefficients in the pontoon y- direction*

Three OrcaFlex models were applied for the global response computation in the detailed correlation work, Xiang and Løken (2023). The main difference between them is what radiation/diffraction results is applied as input: 1-pontoon-model(1PM) using single pontoon results; 3-pontoon-model(3PM) using 3-pontoon interaction results and 10-pontoon-model (10PM) using 10-pontoon full interaction results. Here we present results comparison from 1PM and 3PM. For efficient implementation, 3PM model has been simplified: hydrodynamic interaction problem of three pontoons in the frequency can be solved as usual, but only the self-induced 6x6 added mass and damping coefficients are input to the OrcaFlex model's pontoon hydrodynamics. The 1^{st} and 2^{nd} order wave loads coefficients with full interaction are anyways imported directly into the model. The hydrodynamic coefficients of the pontoon in the middle are input for all the pontoons except for the first and the last pontoon, for which the coefficients from the pontoons on the sides of the three-pontoon model are applied, respectively.

Two long-crested waves are selected as example results in this article:

Wind waves case: Hs=1.8m; Tp=5.5s; Gamma=2.0; Current=0m/s;

Swell waves case: Hs=0.46m; Tp=15.4s; Gamma=4.0; Current=0 m/s;

Three groups of model test results will be included in comparison of the wave tests and simulations. They are test results provided by SINTEF Ocean, postprocessed by NPRA, and measured local wave heights scaled NPRA test results. The linear scaling of results by applying local wave heights is to get some indications only of the local effects of wave height variation on test results. The scaled results are marked with '-Corr' in all the figures of results presented. This is without any interacting global structurally effects considered.

Static tests

The static tests were carried out to verify the static behavior of the installed bridge. This includes deflections of the bridge girder, offsets of the pontoons, and the resulting static loads. Different combinations of loads at different positions were applied on the bridge girder or pontoons during this test, providing a systematic check of different static properties of the installed bridge in the ocean basin. Here example results from one case is given. The test results postprocessed by both NPRA and SO were compared with the NPRA numerical model.

In the example presented, three levels of loads (ranging between 6000 to 12000 kN) were applied on the Pontoon-1 at local coordinates (0, 24.5, 3.5). The static displacements and loads are averaged values from time windows where the model is considered static after initial disturbances of the loading process. The OrcaFlex simulates the same process of loading and postprocessing.

The comparison of results includes the model test results processed by Sintef Ocean(marked with SO), by NPRA (marked with SVV) and computation by NPRA(marked with OF), Figure 24. In some figures the SO results are zero, meaning data missing from the model test reports. The comparison demonstrated that the computations agree very well with the model tests for most of the parameters. However, Pontoon Rz (yaw), girder transverse (y) force, girder transverse (y) and axial (z) motions are not included in the comparison due to their values are too small to demonstrate a reasonable comparison.

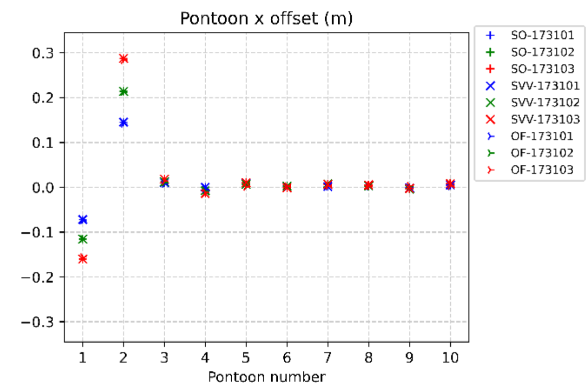

a

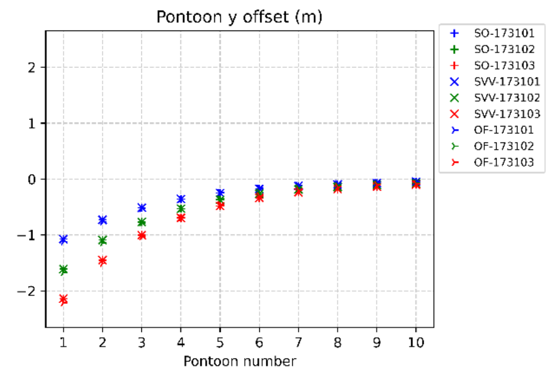

b

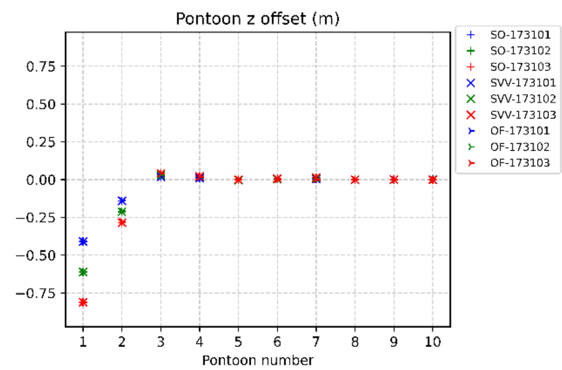

c

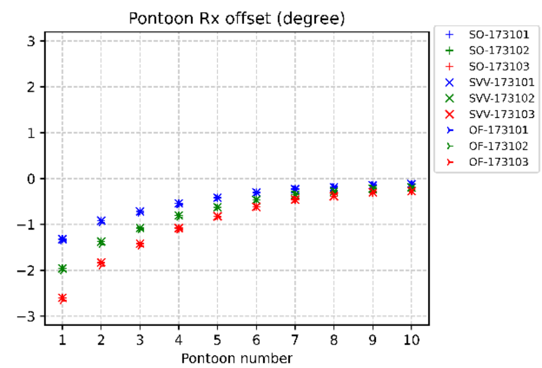

d

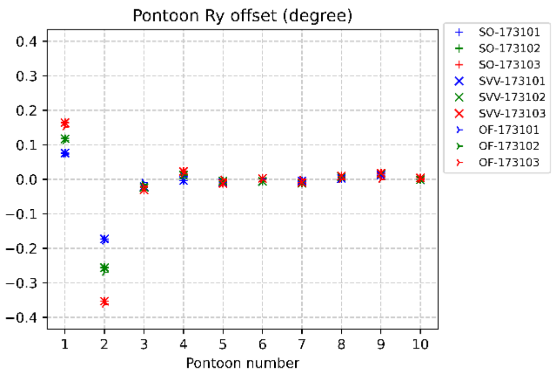
Pontoon Ry offset (degree)
Pontoon number
SO-173101
SO-173102
SO-173103
SVV-173101
SVV-173102
SVV-173103
OF-173101
OF-173102
OF-173103

e

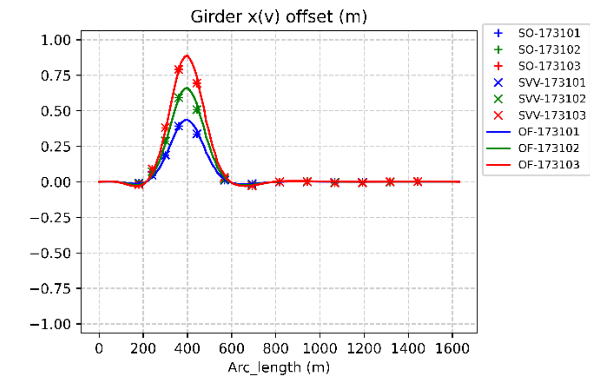
Girder x(v) offset (m)
Arc_length (m)
SO-173101
SO-173102
SO-173103
SVV-173101
SVV-173102
SVV-173103
OF-173101
OF-173102
OF-173103

f

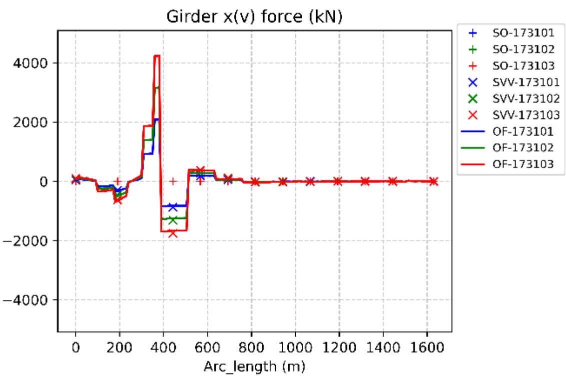
Girder x(v) force (kN)
Arc_length (m)
SO-173101
SO-173102
SO-173103
SVV-173101
SVV-173102
SVV-173103
OF-173101
OF-173102
OF-173103

g

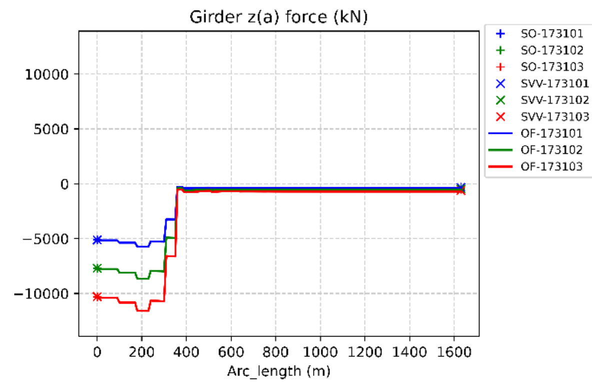
Girder z(a) force (kN)
Arc_length (m)
SO-173101
SO-173102
SO-173103
SVV-173101
SVV-173102
SVV-173103
OF-173101
OF-173102
OF-173103

h

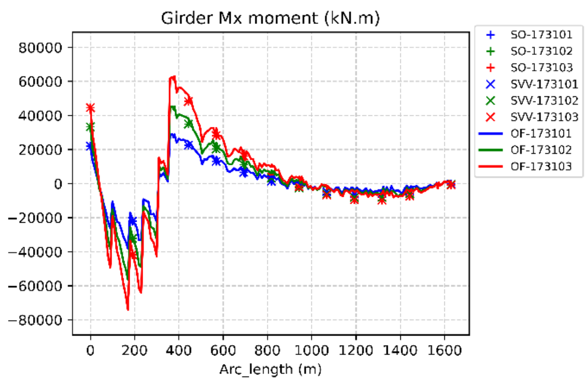
Girder Mx moment (kN.m)
Arc_length (m)
SO-173101
SO-173102
SO-173103
SVV-173101
SVV-173102
SVV-173103
OF-173101
OF-173102
OF-173103

i

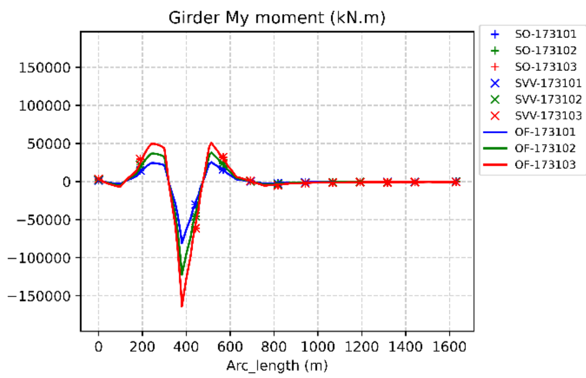
Girder My moment (kN.m)
Arc_length (m)
SO-173101
SO-173102
SO-173103
SVV-173101
SVV-173102
SVV-173103
OF-173101
OF-173102
OF-173103

j

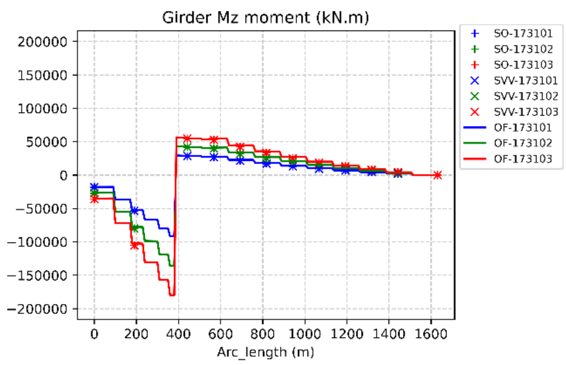
Girder Mz moment (kN.m)
Arc_length (m)
SO-173101
SO-173102
SO-173103
SVV-173101
SVV-173102
SVV-173103
OF-173101
OF-173102
OF-173103

k

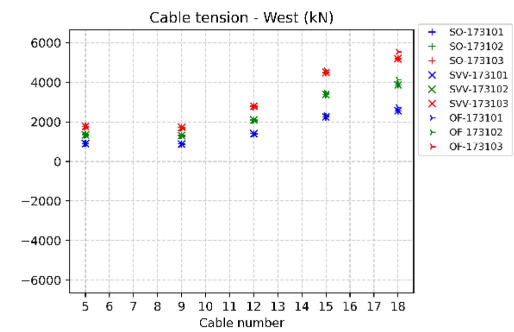
Cable tension - West (kN)
Cable number
SO-173101
SO-173102
SO-173103
SVV-173101
SVV-173102
SVV-173103
OF-173101
OF-173102
OF-173103

l

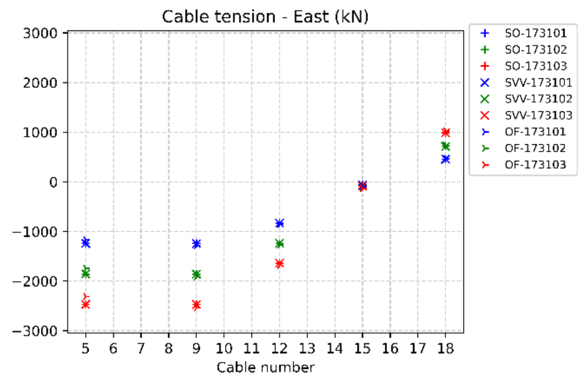

m

Figure 24 *Static (offset) tests of the installed bridge: comparison between model tests and numerical modelling; SO-: SINTEF Ocean model test results; SVV- : NPRA model test results; OF- : NPRA OrcaFlex Simulation; different colors represent different loading levels (tests).*

Decay tests, modal analysis

Decay tests were carried out by pulling bridge girder at specified location (horizontally) and release. The tests were carried out under three different levels (initial displacement of bridge). Analysis of the motion decaying provides the leading natural modes of the bridge. The point of force application is close to the joint of pontoon column-1 and bridge girder, towards the cable-stayed part. The modal analysis of OrcaFlex calculates the undamped modal frequencies and shapes based on standard technique, Orcina (2023).

Table 5 provides a comparison of modes from modal analysis and model tests. There are two groups of modes provided for the OrcaFlex model: Single Pontoon and Interaction. The main difference between them is that if 1PM or 3PM was applied for analysis. One observes that the hydrodynamic interaction affects the modal periods and shapes. The 'Shape' description uses 'T', 'V', 'P', and 'R' to represent main modal shapes observed from the visualized modal shapes from OrcaFlex: (1) 'T': Transverse mode, girder and/or pontoons move in the horizontal plan perpendicular to girder axis; (2) 'R': Rotation mode, girder and/or pontoons rotates around an axis that is (approximately) parallel to the bridge girder; (3) 'V': Vertical mode, girder and pontoons move vertically; (4) 'P': Pendulum mode: pontoon/girder rotates around the axis that is (approximately) perpendicular to the bridge girder. These modal shapes are coupled with other. Thus, the description of mode shape in Table 5 is about the main components that can be observed in the mode shape. The shape components, as described above, are illustrated in Figure 25.

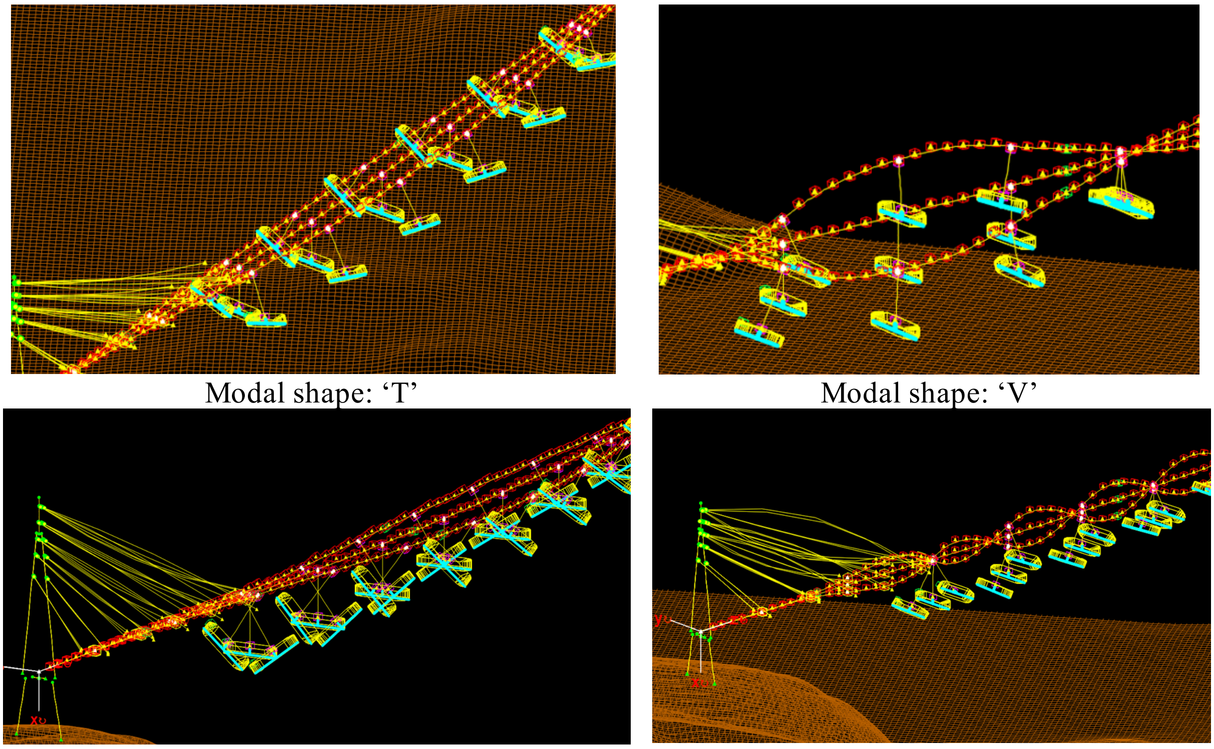

Figure 25 *Modal shapes: the components used to describe a modal shape in Table 5*

Mode number	Model test (FFT/PSD)			OrcaFlex (Single Pontoon)		OrcaFlex (Interaction, 3PM)	
	Period (s)	Diff. (%)		Period (s)	Shape	Period (s)	Shape
1	15.20	1.7	1.7	15.46	T,R	15.47	T, R
2	13.56	2.9	2.9	13.95	T,R	13.95	T, R
3	NA.	NA.	NA.	9.03	T,R	9.03	T, R
4	NA.	NA.	NA.	7.60	T,R	7.61	T,R
5	NA.	NA.	NA.	6.60	T,R	6.84	V,P
6	NA.	NA.	NA.	6.59	V,P,R	6.72	V,P,R
7	NA.	NA.	NA.	6.51	V,R	6.62	V,R
8	NA.	NA.	NA.	6.48	V,P,R	*	*
9	NA.	NA.	NA.	6.32	V,P,R	6.21	V, P
10	NA.	NA.	NA.	5.95	V,P	*	*
11	NA.	NA.	NA.	5.41	V,P	5.26	V,R,P
12	NA.	NA.	NA.	5.17	R,T	5.17	V,P
13	NA.	NA.	NA.	4.82	V,P	4.85	V,P
14	NA.	NA.	NA.	4.29	V,P,R	*	*
15	NA.	NA.	NA.	4.28	R,T	4.28	R,T
16	NA.	NA.	NA.	3.87	V,P	4.07	V,P
17	NA.	NA.	NA.	3.62	R,T	3.62	V,P
18	NA.	NA.	NA.	3.52	V,P	3.49	V,P

Table 5 *Modes of the test bridge model, comparison between (test time series analysis, OrcaFlex modal analysis) (*:missing modes in the interaction model compared with single body model)*

Analysis of the decay tests can obviously extract the first two modes, which are listed in Table 5. The difference between the tests and computations are 1.7% and 2.9% for the first and second modes when single pontoon hydrodynamic coefficients are applied in the numerical model. The interaction model provides almost the same results. For the modal analysis results from single pontoon and interaction models, the first four modes are almost identical, while the deviation starts from the fifth mode. It seems that the 3PM hydrodynamic interaction model catches fewer modes compared with single pontoon model in the period range of (3.5s, 7.0s). A note here is that the process to find the modal periods is manual. Added mass from different periods are input each time and the mode that has the same period as input added mass is identified as a mode. To investigate the reason for this, the diagonal added mass terms with and without hydrodynamic interaction are plotted in Figure 26. It is obvious that A11, A33 and A55 are significantly affected by the hydrodynamic interaction effect when the period is less than 8.0s. The interaction effect is most significant for A11 with even negative added mass for some of the periods. Further, for some oscillations of the added mass there are only one or two frequency points between the peak and trough. This may lead to loss of modes when the manual modal analysis is carried out. It is worth to note that this indicates that increasing the frequency points at lower periods (lower than 7.6 seconds in this case) may improve the hydrodynamic interaction calculation accuracy. However, the 'loss of modes' only means that it is not identified by our analysis, the time domain simulation applies an interpolation strategy on dealing with the discretized frequencies. More detailed study on how much influence this will have on the computation results is undertaken.

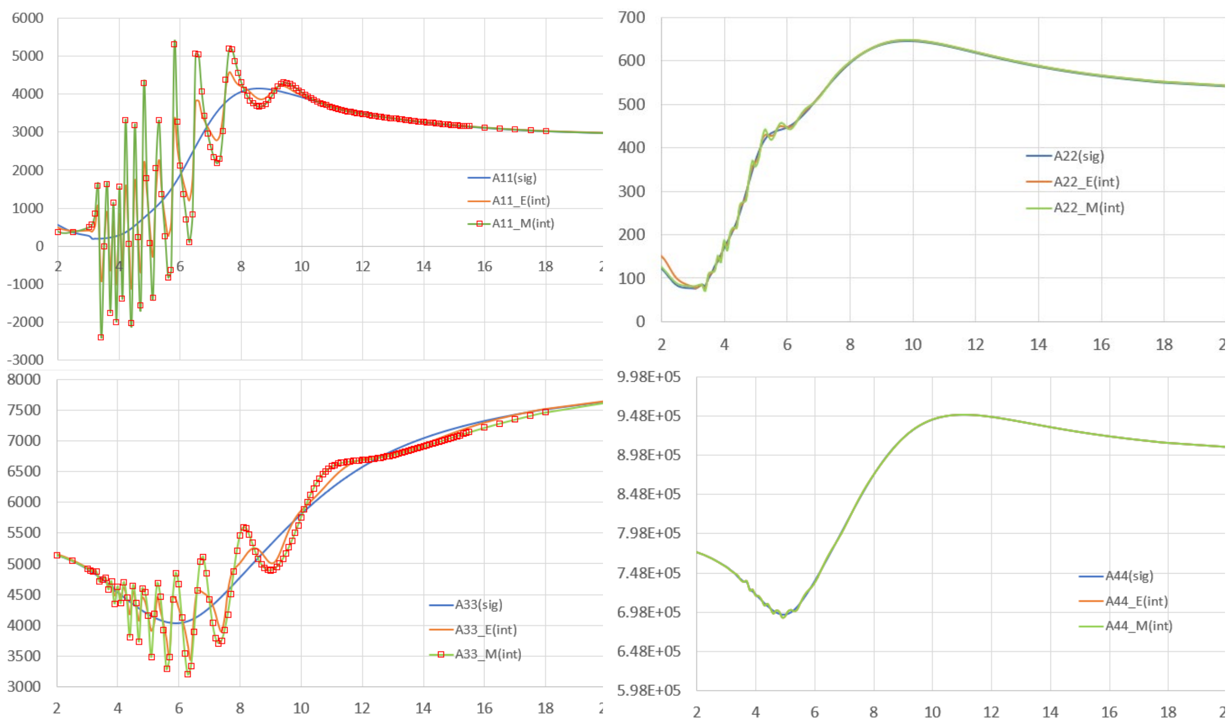

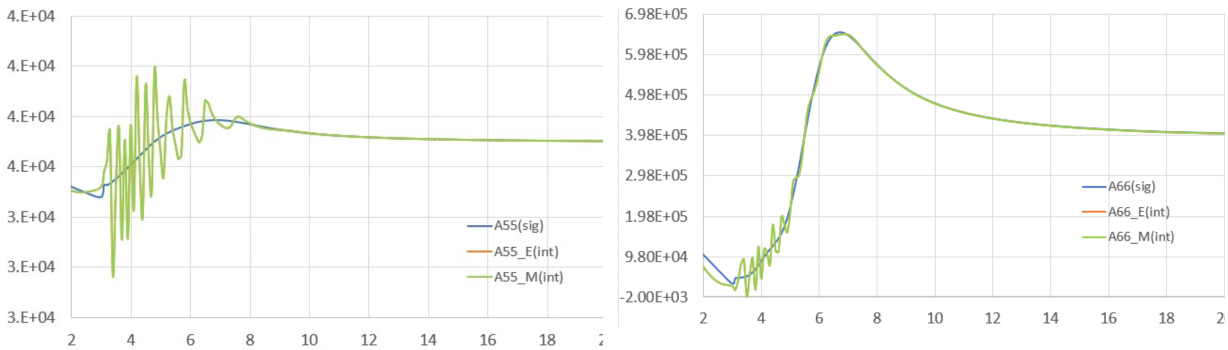

Figure 26 *Comparison: diagonal added mass terms (single pontoon/Sig and mid-pontoon in a three pontoons group/Int) ; _E means the end pontoons and _M the middle pontoons in the hydrodynamic interaction model; horizontal-axis: period(s), vertical-axis: ton or ton*m^2; A11-A33: added mass (moment of inertia) in pontoon x, y, z axis, Figure 4-5; A44-A66: added mass moment of inertia around pontoon x, y, z axis, Figure 4-5;*

The numerical model was also applied to a decay test to simulate in time domain the similar process of loads application and release as the model tests. Selected time series are postprocessed for eigen modes as a confirmation of the modal analysis. The simulation is damped decay carried out with Cd = 0.75 in the pontoon y- direction. Analysis of the y- motion decay time series (1PM model) provides 6 modes (15.50s, 13.98s, 9.05s, 7.63s, 6.64s, 4.30s), which are very close to the non-damped 1PM OrcaFlex model modal analysis. This indicates that the viscous damping has in general small impacts on the eigen modes, and that not all the modes can be identified in one decay simulation. Non-damped modes were used in the comparison in Table 5.

Wind waves test

Comparison of computation with model tests under the wind waves is provided in Figure 28. The wave condition: Hs=1.8m; Tp=5.5s; Gamma=2.0; Current=0m/s; and wave direction is 220 degrees. Figure 27 provides illustration of the bridge model placed in the ocean basin and the location of bridge model under 220 degrees wave/current conditions. It can be observed that most of the pontoons are exposed under this wave direction. Further, due to their small stagers along the wave propagation direction, some pontoons may move in a coordinated way which can enhance the bridge responses.

The comparison shows that numerical model without viscous loads and hydrodynamic interaction leads to in general unsatisfactory comparison. Hydrodynamic interaction has important impact on responses predictions and shall be included in the computation model: this is clearly demonstrated in the comparison of Pontoon x,z and Ry motions and the girder My moment. In contrast, viscous drag helps the comparison towards correct level for response predictions in y, Rx and Rz pontoon motions, transverse (y(t)) girder motion and girder Mx, Mz moments, but trivial effects on x, z, Ry pontoon motions. For cable tensions it is difficult to judge if the viscous drag or hydrodynamic interaction important since no clear trend is observed. However, all the numerical predictions seem to be lower at cables number 15 and 18. The reason may be related to that these two cables are closer to the first ponton column – girder connection and more dynamics are induced in the cables. This will be further investigated.

The comparison for pontoon x, z, and Ry motions, girder vertical x(v) motion My moment are in general not satisfactory for the presented case. These parameters are all hydrodynamic interaction sensitive based on the earlier discussion. Thus, the reasons can be related to that the current hydrodynamic interaction model is not good enough to include all the effects, or other effects like the inhomogeneity of the wave fields along the bridge. Further study is carried out for this issue.

The linear scaling (correction) of model test results by local wave heights from measurements gives no clear conclusion on its improvements on comparison between calculations and test results.

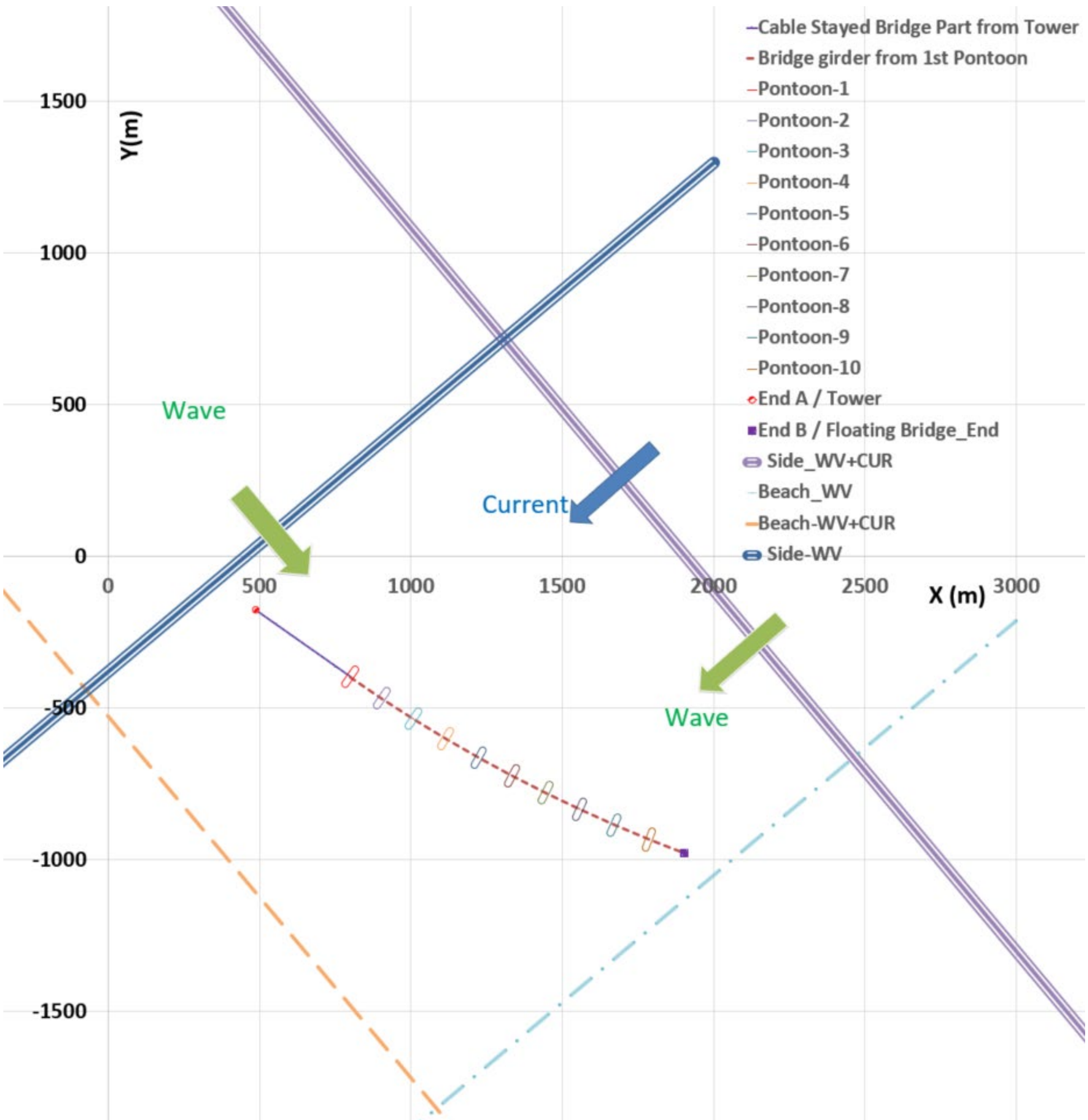

Figure 27 *Illustration of the bridge model placed in the ocean basin; the wave and current direction from the side that generates both waves and current is 220 degrees.*

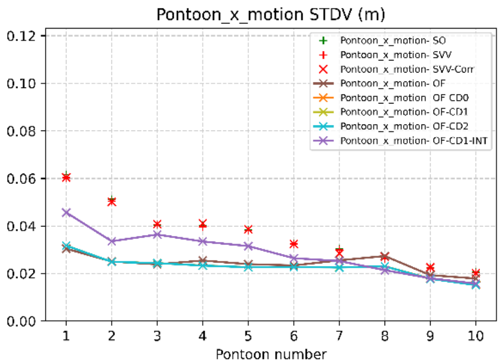
Pontoon_x_motion STDV (m)
Pontoon_x_motion- SO
Pontoon_x_motion- SVV
Pontoon_x_motion- SVV-Corr
Pontoon_x_motion- OF
Pontoon_x_motion- OF-CD0
Pontoon_x_motion- OF-CD1
Pontoon_x_motion- OF-CD2
Pontoon_x_motion- OF-CD1-INT
Pontoon number

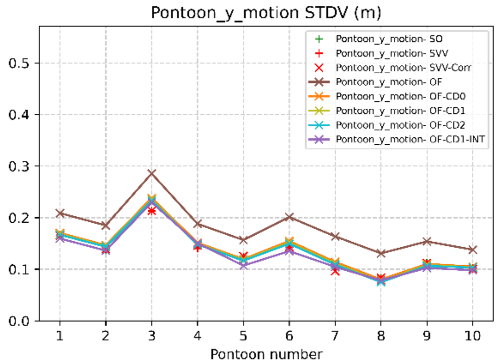
Pontoon_y_motion STDV (m)
Pontoon_y_motion- SO
Pontoon_y_motion- SVV
Pontoon_y_motion- SVV-Corr
Pontoon_y_motion- OF
Pontoon_y_motion- OF-CD0
Pontoon_y_motion- OF-CD1
Pontoon_y_motion- OF-CD2
Pontoon_y_motion- OF-CD1-INT
Pontoon number

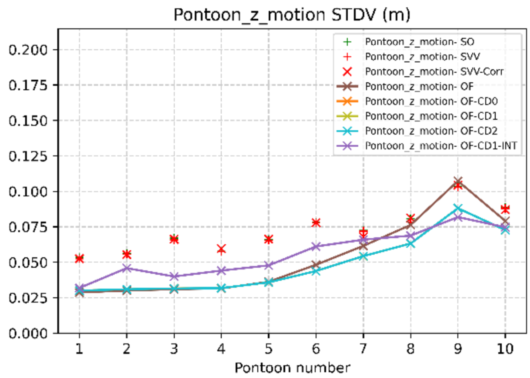
Pontoon_z_motion STDV (m)
Pontoon_z_motion- SO
Pontoon_z_motion- SVV
Pontoon_z_motion- SVV-Corr
Pontoon_z_motion- OF
Pontoon_z_motion- OF-CD0
Pontoon_z_motion- OF-CD1
Pontoon_z_motion- OF-CD2
Pontoon_z_motion- OF-CD1-INT
Pontoon number

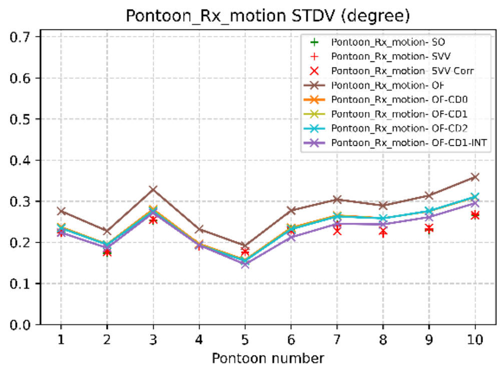
Pontoon_Rx_motion STDV (degree)
Pontoon_Rx_motion- SO
Pontoon_Rx_motion- SVV
Pontoon_Rx_motion- SVV-Corr
Pontoon_Rx_motion- OF
Pontoon_Rx_motion- OF-CD0
Pontoon_Rx_motion- OF-CD1
Pontoon_Rx_motion- OF-CD2
Pontoon_Rx_motion- OF-CD1-INT
Pontoon number

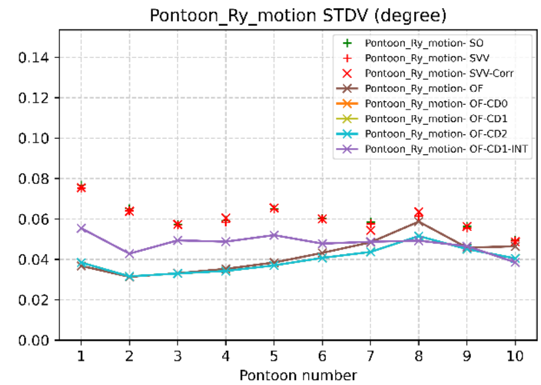
Pontoon_Ry_motion STDV (degree)
Pontoon_Ry_motion- SO
Pontoon_Ry_motion- SVV
Pontoon_Ry_motion- SVV-Corr
Pontoon_Ry_motion- OF
Pontoon_Ry_motion- OF-CD0
Pontoon_Ry_motion- OF-CD1
Pontoon_Ry_motion- OF-CD2
Pontoon_Ry_motion- OF-CD1-INT
Pontoon number

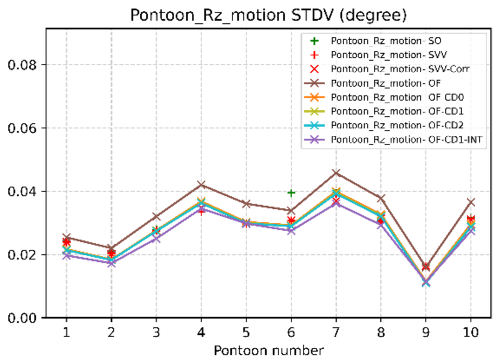
Pontoon_Rz_motion STDV (degree)
Pontoon_Rz_motion- SO
Pontoon_Rz_motion- SVV
Pontoon_Rz_motion- SVV-Corr
Pontoon_Rz_motion- OF
Pontoon_Rz_motion- OF-CD0
Pontoon_Rz_motion- OF-CD1
Pontoon_Rz_motion- OF-CD2
Pontoon_Rz_motion- OF-CD1-INT
Pontoon number

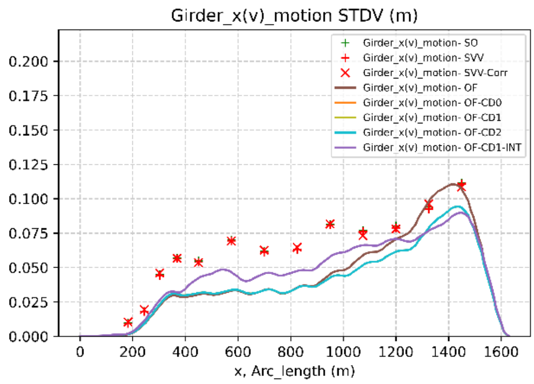
Girder_x(v)_motion STDV (m)
Girder_x(v)_motion- SO
Girder_x(v)_motion- SVV
Girder_x(v)_motion- SVV-Corr
Girder_x(v)_motion- OF
Girder_x(v)_motion- OF-CD0
Girder_x(v)_motion- OF-CD1
Girder_x(v)_motion- OF-CD2
Girder_x(v)_motion- OF-CD1-INT
x, Arc_length (m)

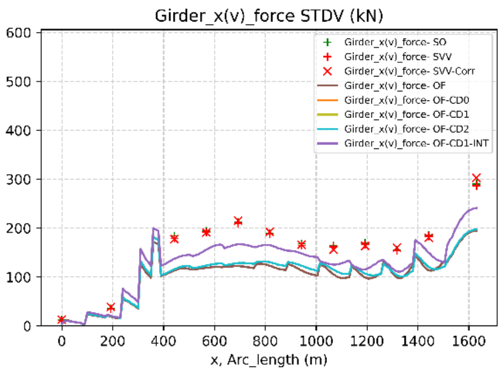
Girder_x(v)_force STDV (kN)
Girder_x(v)_force- SO
Girder_x(v)_force- SVV
Girder_x(v)_force- SVV-Corr
Girder_x(v)_force- OF
Girder_x(v)_force- OF-CD0
Girder_x(v)_force- OF-CD1
Girder_x(v)_force- OF-CD2
Girder_x(v)_force- OF-CD1-INT
x, Arc_length (m)

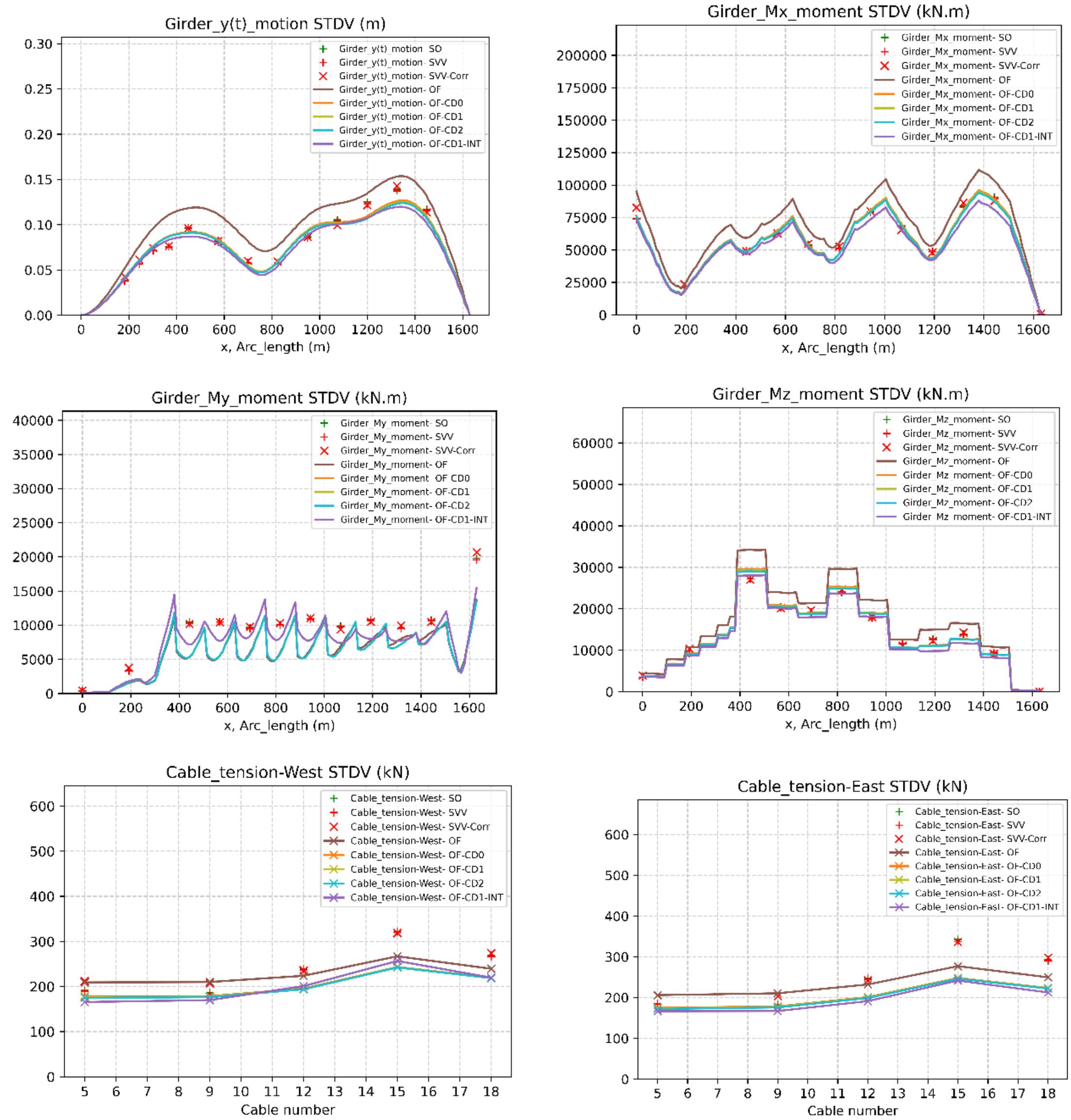

Figure 28 *Wind waves case comparison: all y values given as standard deviation (STDV). Parameter -SO: SINTEF Ocean model test results; Parameter -SVV: NPRA model test results; Parameter -SVV-Corr: NPRA model test results, linearly corrected with local wave heights; Parameter-OF: 1PM OrcaFlex model, Reference Group drag coefficients (Table 4); Parameter-OF-CD0: 1PM OrcaFlex model, CD0 drag coefficients (Table 4); Parameter-OF-CD1: 1PM OrcaFlex model, CD1 drag coefficients (Table 4); Parameter-OF-CD2:1PM OrcaFlex model, CD2 drag coefficients (Table 4); Parameter-OF-CD1-INT:3PM OrcaFlex model, CD1 drag coefficients (Table 4)*

Swell waves test

Figure 29 shows comparison between computation and model tests for different parameters under the swell waves: Hs=0.46m; Tp=15.4s; Gamma=4.0; Current=0 m/s; and wave direction is 220 degrees. Figure 27 provides illustration of the bridge model placed in the ocean basin and the location of bridge model under 220 degrees wave/current conditions. It is observed that most parameters are quite sensitive to that if viscous effect is included in the computation model, but not sensitive to the values of drag coefficients applied. Almost all the parameters are relatively not sensitive to if hydrodynamic interaction effects are included in the computation. Specially, pontoon z, Ry motions and bridge girder vertical x(v) motion are not sensitive to both viscous and hydrodynamic interaction effects. The observations are reasonable. For the first, hydrodynamic interaction effects will be less important at longer periods where the hydrodynamic coefficients are converging with single body coefficients. Most of the oscillations introduced by the hydrodynamic interaction find places under the wave period around 10 seconds, which can be observed in the Figure 11 to Figure 16 for 1st order excitation loads and in Figure 26 for added mass coefficients. For the second, the significant difference of responses with and without viscous drag loads included proves that the main damping source in the swell region comes from the viscous damping since the potential damping approaches zero at and beyond the swell region; or in other words, trivial wave generation happens when the pontoons are under forced motions of swell wave periods.

As in the wind waves tests, the linear scaling (correction) of model test results by local wave heights from measurements gives no clear conclusion on its improvements on comparison between calculations and test results.

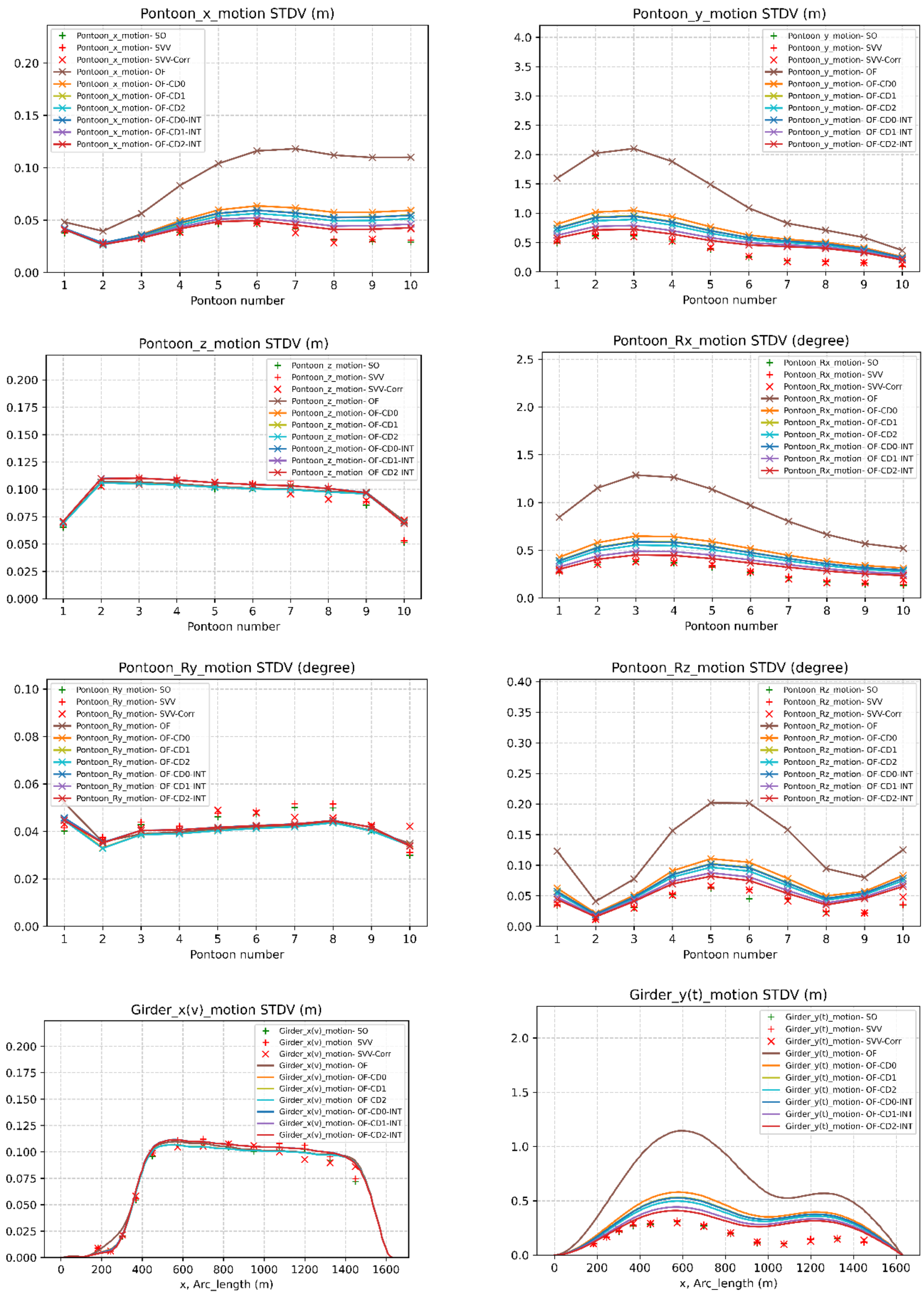

Pontoon_x_motion STDV (m)
Pontoon_x_motion- SO
Pontoon_x_motion- SVV
Pontoon_x_motion- SVV-Corr
Pontoon_x_motion- OF
Pontoon_x_motion- OF-CD0
Pontoon_x_motion- OF-CD1
Pontoon_x_motion- OF-CD2
Pontoon_x_motion- OF-CD0-INT
Pontoon_x_motion- OF-CD1-INT
Pontoon_x_motion- OF-CD2-INT
Pontoon number
Pontoon_y_motion STDV (m)
Pontoon_y_motion- SO
Pontoon_y_motion- SVV
Pontoon_y_motion- SVV-Corr
Pontoon_y_motion- OF
Pontoon_y_motion- OF-CD0
Pontoon_y_motion- OF-CD1
Pontoon_y_motion- OF-CD2
Pontoon_y_motion- OF-CD0-INT
Pontoon_y_motion- OF-CD1-INT
Pontoon_y_motion- OF-CD2-INT
Pontoon number
Pontoon_z_motion STDV (m)
Pontoon_z_motion- SO
Pontoon_z_motion- SVV
Pontoon_z_motion- SVV-Corr
Pontoon_z_motion- OF
Pontoon_z_motion- OF-CD0
Pontoon_z_motion- OF-CD1
Pontoon_z_motion- OF-CD2
Pontoon_z_motion- OF-CD0-INT
Pontoon_z_motion- OF-CD1-INT
Pontoon_z_motion- OF-CD2-INT
Pontoon number
Pontoon_Rx_motion STDV (degree)
Pontoon_Rx_motion- SO
Pontoon_Rx_motion- SVV
Pontoon_Rx_motion- SVV-Corr
Pontoon_Rx_motion- OF
Pontoon_Rx_motion- OF-CD0
Pontoon_Rx_motion- OF-CD1
Pontoon_Rx_motion- OF-CD2
Pontoon_Rx_motion- OF-CD0-INT
Pontoon_Rx_motion- OF-CD1-INT
Pontoon_Rx_motion- OF-CD2-INT
Pontoon number
Pontoon_Ry_motion STDV (degree)
Pontoon_Ry_motion- SO
Pontoon_Ry_motion- SVV
Pontoon_Ry_motion- SVV-Corr
Pontoon_Ry_motion- OF
Pontoon_Ry_motion- OF-CD0
Pontoon_Ry_motion- OF-CD1
Pontoon_Ry_motion- OF-CD2
Pontoon_Ry_motion- OF-CD0-INT
Pontoon_Ry_motion- OF-CD1-INT
Pontoon_Ry_motion- OF-CD2-INT
Pontoon number
Pontoon_Rz_motion STDV (degree)
Pontoon_Rz_motion- SO
Pontoon_Rz_motion- SVV
Pontoon_Rz_motion- SVV-Corr
Pontoon_Rz_motion- OF
Pontoon_Rz_motion- OF-CD0
Pontoon_Rz_motion- OF-CD1
Pontoon_Rz_motion- OF-CD2
Pontoon_Rz_motion- OF-CD0-INT
Pontoon_Rz_motion- OF-CD1-INT
Pontoon_Rz_motion- OF-CD2-INT
Pontoon number
Girder_x(v)_motion STDV (m)
Girder_x(v)_motion- SO
Girder_x(v)_motion- SVV
Girder_x(v)_motion- SVV-Corr
Girder_x(v)_motion- OF
Girder_x(v)_motion- OF-CD0
Girder_x(v)_motion- OF-CD1
Girder_x(v)_motion- OF-CD2
Girder_x(v)_motion- OF-CD0-INT
Girder_x(v)_motion- OF-CD1-INT
Girder_x(v)_motion- OF-CD2-INT
x, Arc_length (m)
Girder_y(t)_motion STDV (m)
Girder_y(t)_motion- SO
Girder_y(t)_motion- SVV
Girder_y(t)_motion- SVV-Corr
Girder_y(t)_motion- OF
Girder_y(t)_motion- OF-CD0
Girder_y(t)_motion- OF-CD1
Girder_y(t)_motion- OF-CD2
Girder_y(t)_motion- OF-CD0-INT
Girder_y(t)_motion- OF-CD1-INT
Girder_y(t)_motion- OF-CD2-INT
x, Arc_length (m)

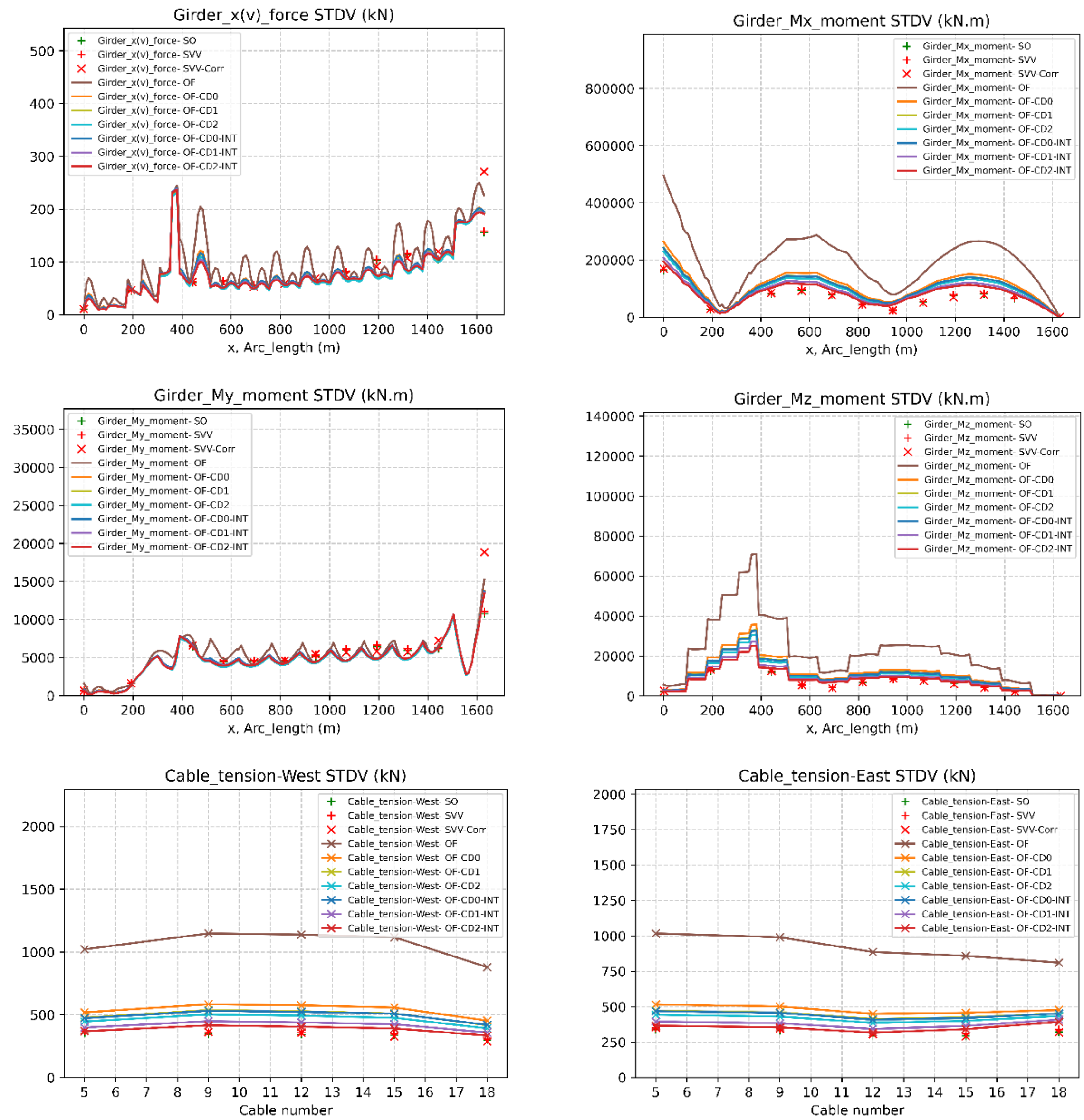

Figure 29 *Swell waves case comparison: all y values given as standard deviation (STDV). Parameter -SO: SINTEF Ocean model test results; Parameter -SVV: NPRA model test results; Parameter -SVV-Corr: NPRA model test results, linearly corrected with local wave heights; Parameter-OF: 1PM OrcaFlex model, Reference Group drag coefficients (Table 4); Parameter-OF-CD0: 1PM OrcaFlex model, CD0 drag coefficients (Table 4); Parameter-OF-CD1: 1PM OrcaFlex model, CD1 drag coefficients (Table 4); Parameter-OF-CD2:1PM OrcaFlex model, CD2 drag coefficients (Table 4); Parameter-OF-CD0-INT:1PM OrcaFlex model, CD0 drag coefficients (Table 4); Parameter-OF-CD1-INT:1PM OrcaFlex model, CD1 drag coefficients (Table 4); Parameter-OF-CD2-INT:1PM OrcaFlex model, CD2 drag coefficients (Table 4)*

Concluding remarks

The model tests together with correlation analysis have laid solid basis for further design and analysis. The tests and results can be used as basis and reference for further engineering design of the floating bridge crossing the Bjørnafjord. The tests were carried out for either one or three pontoons or a truncated bridge which is approximately 1/3 of the full bridge. Extrapolation of results and conclusions from that of the truncation model to the full bridge is straightforward for most of the loads and responses excited by waves and current since what is in common here is the numerical strategies and tools (software); and validation of the tools is a central topic in the tests and correlation work. However, it is still important to keep in mind that the some of the first modes (periods longer than 16.0 second in this test) of the full bridge are missing in the model tests, which was proved by earlier analysis (during the model test design phase) to be not of critical importance for the work scope of the test project.

The tests and comparison showed that hydrodynamic interaction effects shall be accounted for in the computation of the tested floating bridge. This has also proved our earlier report in Xiang et. al. (2018) and Fenerci et.al. (2022). Further, the comparison also showed that the hydrodynamic interaction model works not satisfactorily under certain cases, thus further improvement shall be carried out. An investigation showed that modal analysis may miss important modes due to the highly oscillatory added mass coefficients at short wave region, and this issue is now further studied.

The implementation of viscous loads in the form of Morison-type drag term is important for improving comparison under both wind waves and swell conditions, while of special importance for avoiding overestimating most of responses under swell waves. One must note that this implementation may not work correctly for combined wave-current cases, where a damping effect may be demonstrated for the bridge responses, while all the model tests we have gone through indicate bridge responses increase under such conditions. This was emphasized in Løken and Xiang (2018), Xiang and Løken (2019a, 2019b), and our new computations of the new tests also proved this, Xiang and Løken (2023).

An important observation in the model tests and comparison work is that the impact of current on the bridge loads and responses when combined with waves. Groups of waves combined with current under the same direction were tested for both the pontoons and the high bridge. The increased responses under tested wave-current conditions proved our earlier report in Løken and Xiang (2018), Xiang and Løken (2019a, 2019b). This is an issue that requires careful investigation and knowledge development before we can conclude, thus we select to only report zero current results here. Our recent study has demonstrated that one shall focus on implementing the changed dispersion equation due to refraction of waves running on a current, and its impact on hydrodynamic coefficients of a pontoon and relative phases between pontoons. Further, shortcrestedness of waves has practical importance for the impact of this effect on floating bridge design, Fredriksen and Kvåle (2023), Faltinsen (2023), Xiang (2023).

The wave inhomogeneity in the model basin and its impact on test results is one uncertainty that should be further studied. The input waves to the simulations were calibrated at the center of the basin, while the bridge pontoons are distributed over the whole basin. Thus, for some cases corrections may be needed for the wave conditions. The correction may be made for: (1) The wave height at a pontoon; (2) The wave direction at a pontoon; (3) The wave period at a pontoon. Observation has shown that the wave periods are mostly consistent over all the locations where the pontoons are placed. Thus, the corrections can be made for both the wave height and directions. It is a very challenging task to identify the local wave directions in the model tests, while wave height correction seems easier to be implemented. Further, it was demonstrated in the wave tests comparison that the wave heights correction shall be included in the structural dynamics system analysis, since simple scaling of results by local wave heights provides no improvement of comparison.

Acknowledgements

For this series of floating bridge model tests work: Dr. Arne Edvin Løken as the technical adviser, Dr. Ole Anton Grytå as the project administration and technical reviewer; Prof. em. William C. Webster (UC Berkely), Prof. em. Preben Terndrup Pedersen (DTU), Dr. Guy Larose (RWDI) as expert group for technical input, workshops, and discussion on different topics. Model test team at SINTEF Ocean for their excellent model tests implementation and data analysis; among others: Dr. Thomas Viuff, Dr. Ole David Økland, Dr. Senthuran Ravinthrakumar, Dr. Hagbart Alsos and Dr. Halvor Lie.

References

1. Engineering News-Record (2018) The 10 Longest Floating Bridges in the World. Available online: https://www.enr.com/articles/44013-the-10-longest-floating-bridges-in-the-world (accessed on 19.12.2020).
2. Mellbye, C.S., Amble, I.B., Fjose, S. (2015) Eksport fra norske regioner - et regionalt perspektiv på norsk eksportvirksomhet. Menon Business Economics Report, in Norwegian.
3. Fredriksen,A., Kvåle, K.A. (2023) Investigation of wave-current interaction and recommended methodology for inclusion in global design analysis, Doc number 10205546-09-NOT-303, technical notes from AMC to Statens vegvesen.
4. Giske, J. H. (2019). Optimizing pontoon spacing for floating bridge over Bjørnafjorden; Master thesis, Lund University, Sweden.
5. Statens vegvesen (2017) Grensesprengande brubygging. Available online: https://www.vegvesen.no/Europaveg/e39stordos/nyhetsarkiv/grensesprengande-brubygging (accessed on 19.12.2020).
6. Regjeringen (The Norwegian Government) (2017). Langsiktig mål om ferjefri E39. Available online: https://www.regjeringen.no/no/aktuelt/langsiktig-mal-om-ferjefri-e39/id2548526/ (accessed on 19.12.2020).
7. Statens vegvesen (2020) NTP-svar fra Vegvesenet. Prosjektene som gir mest positiv nytte for trafikantene. Available online: https://www.vegvesen.no/om-oss/presse/aktuelt/nasjonalt/ntp-for-2022-2033/ (accessed on 08.01.2023).
8. Aas-Jakobsen (2020) Unik kobling av flytebru og skråstagsbru. Available online: https://www.aaj.no/prosjekter/nordhordlandsbrua/ (accessed on 19.12.2020).
9. DNV (2014) Recommended practice DNV-RP-C205, Det Norsk Veritas, Norway.
10. Faltinsen, O. M. (2005) *Hydrodynamics of high-speed marine vehicles*. Cambridge university press.
11. Faltinsen, O.M. (2023) Series of personal communication about wave-current-structure interaction for floating bridge loads and responses, in emails and so on.
12. Fenerci, A., Kvåle, K. A., Xiang, X., & Øiseth, O. (2022). Hydrodynamic interaction of floating bridge pontoons and its effect on the bridge dynamic responses. Marine Structures, 83, 103174.
13. Statens vegvesen, "SBJ-01-C4-SVV-01-BA-001 MetOcean Specification Rev. 2B," 28.01.20.
14. Rodrigues, J.M., Viuff, T., Økland, O.D., (2022). Model tests of a hydroelastic truncated floating bridge. Applied Ocean Research 125, 103247. doi: 10.1016/j.apor.2022.103247.
15. Shao, Y., Xiang, X., & Liu, J. (2019). Numerical investigation of wave-frequency pontoon responses of a floating bridge based on model test results. In International Conference on Offshore Mechanics and Arctic Engineering (Vol. 58769, p. V001T01A019). American Society of Mechanical Engineers.
16. Sintef Ocean (2021a), "SBJ-32-C5-SINT-21-RE-001-0 Bjørnafjorden hydrodynamic tests - 1 pontoon", 2021.

17. Sintef Ocean (2021b) SBJ-32-C5-SINT-21-RE-002-0 Bjørnafjorden hydrodynamic tests - 3 pontoons. Sintef Ocean Report, Trondheim, Norway.
18. Sintef Ocean (2021c) SBJ-32-C5-SINT-21-RE-003-0 SVV High Bridge Model Tests. Sintef Ocean Report, Trondheim, Norway.
19. Sintef Ocean (2022) "Ocean Laboratory", https://www.sintef.no/en/all-laboratories/ocean-laboratory/; accessed 12.2022.
20. Standard Norge (2017) NORSOK N-003:2017: Actions and action effects.
21. Statens vegvesen (2022) "SBJ-01-C4-SVV-01-BA-001 MetOcean Specification. Rev. 2D", Statens vegvesen report.
22. Svendsen, I. A. (2005). Introduction to nearshore hydrodynamics (Vol. 24). World Scientific Publishing Company.
23. Orcina (2022) OrcaWave ver.11.2.
24. Orcina (2022) OrcaFlex ver.11.2.
25. ANSYS(2020) AQWA ver.2020 R2.
26. Løken, A., Oftedal, R., Aarsnes, J. (1990) Aspects of hydrodynamic loading and response in design of floating bridges. Second Symposium on Strait Crossings, 479–486.
27. Løken, A., Xiang, X. (2018) "SBJ-32-C4-SVV-21-TN-002, Memo to engineering consultants in phase 5 for Bjørnafjorden floating bridge hydro elastic dynamics in design", Staten vegvesen Report.
28. Ravinthrakumar, S., Alsos, H., Økland, O.D., Lie, H., Xiang, X., Grytå, O.A., (2023a) Forced motion of a floating bridge pontoon to evaluate the hydrodynamic damping properties. Applied Ocean Research, Submitted.
29. Ravinthrakumar, S., Alsos, H., Økland, O.D., Lie, H., Xiang, X., Grytå, O.A., (2023b) Global Responses and Hydrodynamic Loads on Pontoons in Regular and Irregular Waves. Applied Ocean Research, Submitted.
30. Viuff, T., Xiang, X., Leira, B. J., & Øiseth, O.(2020a). Software-to-software comparison of end-anchored floating bridge global analysis, Bridge Engineering, vol. 25(5), pp. 04020022. doi:10.1061/(ASCE)BE.1943-5592.0001545.
31. Viuff, T., Xiang, X., Øiseth, O., & Leira, B. J. (2020b). Model uncertainty assessment for wave-and current-induced global response of a curved floating pontoon bridge. Applied Ocean Research, 105, 102368.
32. Viuff, T. (2020). "Uncertainty assessment of wave- and current-induced global response of floating bridges - A numerical investigation», Ph.D. thesis. Norwegian University of Science and Technology. Trondheim, Norway. URL: https://hdl.handle.net/11250/2651104.
33. Viuff, T., Ravinthrakumar, S., Økland, O. D., Grytå, O. A., & Xiang, X. (2023a). Model test of a hydroelastic truncated floating bridge with a stay-cable tower. Applied Ocean Research, 135, 103539.
34. Viuff, T., Ravinthrakumar, S., Økland, O. D., Grytå, O. A., & Xiang, X. (2023b) Experimental study of floating bridge global response when subjected to waves and current. Applied Ocean Research, Submitted.
35. Xiang, X., Svangstu, E., Nedrebø, Ø., Jakobsen, B., Eidem, M. E., Larsen, P. N., & Sørby, B. (2017). Viscous damping modelling of floating bridge pontoons with heaving skirt and its impact on bridge girder bending moments. In International Conference on Offshore Mechanics and Arctic Engineering (Vol. 57748, p. V07BT06A001). American Society of Mechanical Engineers.
36. Xiang, X., Viuff, T., Leira, B., & Øiseth, O. (2018). Impact of hydrodynamic interaction between pontoons on global responses of a long floating bridge under wind waves. In International Conference on Offshore Mechanics and Arctic Engineering (Vol. 51265, p. V07AT06A049). American Society of Mechanical Engineers.
37. Xiang, X., Løken, A. (2019a). Hydro-elastic analysis and validation of an end-anchored floating bridge under wave and current loads. In International Conference on Offshore Mechanics and Arctic Engineering (Vol. 58882, p. V009T12A018). American Society of Mechanical Engineers.
38. Xiang, X., Løken, A. (2019b). "SBJ-32-C4-SVV-21-RE-001, Floating bridge hydro elastic model tests: re-modelling past tests and planning new tests", Statens vegvesen report.
39. Xiang, X., Løken, A. (2020a) " SBJ-32-C5-SVV-21-RE-001-0 Floating bridge hydrodynamic model tests specification 1 – Single pontoon", Statens vegvesen report.
40. Xiang, X., Løken, A. (2020b) "SBJ-32-C5-SVV-21-RE-002-0 Floating bridge hydrodynamic model tests specification 2 – Three pontoons", Statens vegvesen report.
41. Xiang, X., Løken, A. (2020c) "SBJ-32-C5-SVV-21-RE-003-0 Floating bridge hydrodynamic model tests specification 3 – High bridge tests", Statens vegvesen report.
42. Xiang, X., Løken, A. (2023) "SBJ-32-C6-SVV-21-TN-001-0, Technical notes: Floating bridge hydrodynamics model tests 2020 – 2021", Statens vegvesen report.
43. Xiang, X. (2023) "Wave-current interaction of floating bridge hydrodynamics – experience from model tests", Technical notes to Standard Norge (Standards Norway), unpublished.